
Article:
Yang, D., Liu, F., Huang, S.-S. orcid.org/0000-0003-2816-7104 et al. (1 more author) (2021) Fire performance of eccentrically-loaded square and rectangular tubed-reinforced-concrete columns. Structures, 33. pp. 1053-1076. ISSN 2352-0124

https://doi.org/10.1016/j.istruc.2021.04.080

Fire performance of eccentrically-loaded square and rectangular tubed-reinforced-concrete columns

Dongdong Yang [a,b], Faqi Liu [a,b,*], Shan-Shan Huang [c], Hua Yang [a,b]

[a] *Key Lab of Structures Dynamic Behaviour and Control (Harbin Institute of Technology), Ministry of Education, Heilongjiang, Harbin 150090, China*

[b] *Key Lab of Smart Prevention and Mitigation of Civil Engineering Disasters (Harbin Institute of Technology), Ministry of Industry and Information Technology, Heilongjiang, Harbin 150090, China*

[c] *Department of Civil and Structural Engineering, The University of Sheffield, Sir Frederick Mappin Building, Mappin Street, Sheffield S1 3JD, UK*

---

* Corresponding author:

Faqi Liu

Key Lab of Structures Dynamic Behaviour and Control (Harbin Institute of Technology), Ministry of Education & Key Lab of Smart Prevention and Mitigation of Civil Engineering Disasters (Harbin Institute of Technology), Ministry of Industry and Information Technology, Harbin 150090, China;

Tel: +86-451-86286962

Email: fqliu@hit.edu.cn (F. Liu)

Abstract

Tubed-reinforced-concrete (TRC) columns are gaining increasing popularity in engineering constructions, however, research on their fire performance is still limited and mainly focused on concentrically-loaded columns. In this study, extensive numerical analysis was carried out to investigate the performance of square and rectangular TRC columns under eccentric loading and exposed to ISO 834 standard fire. A sequentially-coupled thermo-mechanical finite element analysis (FEA) model was developed in ABAQUS and validated well against fire testing results. The high-temperature overall deformations, internal bending moments and cross-sectional load redistributions of square TRC columns with different load eccentricities were analysed. Parametric studies were conducted to investigate the influences of load eccentricity ratio, sectional aspect ratio, bending direction, fire protection thickness, sectional dimension, load ratio and slenderness ratio on the fire resistance of square and rectangular TRC columns. Load eccentricity was found to have a greater effect on the fire resistances of columns of lower slenderness than those of columns of higher slenderness. Rectangular TRC columns of sectional aspect ratios no larger than 2 could generally achieve identical buckling resistance as that of the equivalent square sections. The influences of sectional aspect ratio and bending direction on the column fire resistance were insignificant. A design method was then proposed for both the ambient-temperature and high-temperature designs of eccentrically-loaded square and rectangular TRC columns. The fire design method could cover both protected and unprotected TRC columns. The design method has been thoroughly validated against detailed FEA modelling and yields excellent agreements with the modelling results.

Keywords: Tubed-reinforced-concrete (TRC) columns; Eccentric load; Fire resistance; Fire protection; Design method.

1. Introduction

Tubed-reinforced-concrete (TRC) columns, also known as steel tube confined reinforced concrete (STCRC) columns, is an innovate type of steel-concrete composite column that consists of outer steel tube, inner concrete core and reinforcing bars. Commonly-used cross-sectional shapes of TRC columns are circular, square and rectangular. Being terminated at the beam-column connections, the steel tube in TRC columns is designed to mainly provide confinement to inner concrete, as shown in Fig. 1. Unlike conventional concrete-filled steel tubular (CFST) columns in which the steel tube is under axial compression and transverse tension, the steel tube of TRC columns is designed to take transverse tension only. Compared to CFST columns, local buckling of steel tube could generally be prevented or delayed in TRC columns [1-3] and so much thinner steel tubes could be used.

Tomii et al. [4, 5], for the first time, proposed the concept of TRC columns to improve the shear strength and seismic performance of reinforced concrete (RC) columns. Over the past few decades, extensive studies have been conducted to investigate the static and seismic performance of TRC columns, both experimentally and numerically [6-15]. Ambient-temperature design guidelines of TRC columns are currently available in the Chinese standard JGJ/T471 [16]. Thanks to their advantages, such as high bearing capacity, good ductility, excellent seismic performance and ease of construction, TRC columns are gaining increasing popularity in the constructions of high-rise buildings and large-span stadiums in China [17].

Structural fire safety design is essential for column members, since column failure in fire could lead to severe overall structural collapse and cause great losses of lives. However, a fire design method for TRC columns is still unavailable in current design standards as far as the authors know. The authors have carried out extensive experimental investigations and numerical studies on the performance of TRC columns during and after the exposure to fire, to develop practical high-temperature design methods for TRC columns of circular cross-section [18-20] and square and

rectangular sections [17, 21-23]. In particular, Yang et al. [23] have developed a simplified method for the fire resistance design of square and rectangular TRC columns under concentric load based on extensive parametric studies on both unprotected and protected columns.

Most of columns are subject to the combined effects of compression and bending in reality, therefore, it is necessary to consider eccentric-loading in column design. Research and design method for eccentrically-loaded square and rectangular TRC columns exposed to fire are still lacking. FEA modelling is conducted in this study to investigate the fire performance of square and rectangular TRC columns with and without fire protection subject to eccentric load. The influences of load ratio, load eccentricity ratio, cross-sectional dimension, slenderness ratio, cross-sectional aspect ratio, bending direction and fire protection thickness on the deformation behaviour and fire resistance are analysed. Based on the results of parametric studies, a practical method is proposed for the fire resistance design of unprotected and protected square and rectangular TRC columns under eccentric loading.

2. FEA modelling

The FEA model is established using the sequentially-coupled temperature-displacement modelling procedure of ABAQUS. A heat transfer analysis is firstly conducted; the output nodal temperatures are then input into the mechanical analysis. Identical meshing is, therefore, adopted in the heat transfer and mechanical models. The loading and geometry symmetries allow the modelling of only half of the column by using symmetric boundary conditions, as shown in Fig. 2. A mesh sensitivity study is conducted for both the thermal and structural analyses, confirming that 14 elements on the column edge along the x axis in Fig. 2 are sufficient.

2.1 Heat transfer analysis

It is assumed that each model is exposed to the ISO 834 [24] standard fire at all four

faces along the entire column length. The convection coefficient and emissivity recommended in EC4 [25], 25 W/(m^2·K) and 0.7, respectively, are applied onto the heated surfaces. The temperature-dependent thermal properties of concrete and steel, e.g. thermal conductivity and specific heat, recommended by Lie [26], are used. The latent heat of water vaporization in the concrete core is considered using the modification method proposed by Han [27], where the moisture content is assumed as 5%. A thermal resistance of 100 W/(m^2·K) recommended by Ding and Wang [28] is applied to the steel tube-concrete interface. It is assumed that the rebar temperature is the same as the adjacent concrete temperature, and so the rebars' nodes are tied to the correlating concrete nodes. The heat transfer elements DC3D8, DS4 and DC1D2 of ABAQUS are used to model concrete, steel and rebars, respectively.

For the modelling of protected columns, sprayed cementitious material is adopted as the fire protection. The inner surface of the fire protection is tied to the outer surface of the steel tube. Element type DC3D8 is used to model the fire protection, which has the same mesh as for the steel tube. It should be noted that the thermal properties of the protection material, e.g. thermal conductivity and specific heat, vary with temperature. However, it is difficult to obtain these thermal properties at elevated temperatures through experiments and the measured values are highly affected by the test methods, environmental conditions and the chemical compositions of the material itself. Information on the temperature-dependent thermal properties of sprayed protection materials is still limited. For the ease of conducting extensive analysis and engineering design, the thermal properties of the protection material are usually assumed to be constant in practice, such as the provisions in the Chinese design code GB 51249 [29], the numerical modelling conducted by Han et al. [27, 30], Xiong [31], Wang and Li [32], Li et al. [33] and Ren et al. [34] and the fire design methods of protected members developed in references [35-39]. This simplified approach has been proved sufficient to represent the effect of sprayed fire protection on the temperature of heated members [29]. Therefore, constant thermal properties of the fire protection, i.e. conductivity 0.116 W/(m·°C), specific heat 1024 J/(kg·°C) and density

400 kg/m^3, recommended by the Chinese code GB 50936 [40], are used in this paper.

2.2 Mechanical analysis

As noted, Fig. 2 illustrates the mechanical FEA model. As noted in Section 1, the steel tube of a TRC column is cut close to the column-beam joints, so that the steel tube does not directly bear the axial load. This paper concentrates on the fire performance of isolated TRC columns and so the joint is not modelled. To ensure that the axial load is not directly applied to the steel tube, the top and bottom ends of the inner RC section are modelled with rigid bodies with corresponding reference points RP1 and RP2. A constant eccentric load N_f is applied on to RP1, which is at a distance e from the section centre. The boundary conditions at the top and bottom ends of the column are imposed to RP1 and RP2, respectively.

The concrete damage plasticity (CDP) model of ABAQUS, the compressive stress-strain relationship of concrete recommended by Lie [26] and the tensile constitutive model of concrete suggested by Hong and Varma [41] are adopted to model the concrete core. The thermal expansion coefficient of concrete is assumed to be constant during heating, which is 6×10^{-6}/°C, as adopted by Yang et al. [17, 23], Liu et al. [20], Hong and Varma [41] and Espinos et al. [42]. The EC4 [25] material models of structural steel and steel rebars are used to model the steel tube and reinforcing bars. Coulomb friction with a coefficient of 0.3 and hard contact are used to simulate the surface-to-surface interactions at the steel tube-concrete interface. It is assumed that there is no slip between the rebars and concrete core. Therefore, the reinforcing bars are embedded into the concrete core in the FEA to achieve deformation compatibility. The initial global imperfection is assumed to be L/1000 following the first buckling mode, where L is the column length. The element types C3D8R, S4R and T3D2 of ABAQUS are used for concrete, steel tube and rebars, respectively. The fire protection is not included in the mechanical analysis, whereas it is included in the thermal analysis. The major- and minor-axis bending of rectangular columns are investigated separately and the two-way buckling failure caused by the interaction

between major- and minor-axis bending is not considered.

2.3 Model validation

By far, 11 fire tests have been conducted on TRC columns, including four circular columns [20], five square columns [17] and two rectangular columns [23]. All these tests have been modelled to calibrate the FEA model developed by the authors [17, 23]. The FEA predicted axial deformation-time relationships, lateral deformation-time relationships, failure modes and fire resistance of the tested TRC specimens agree well with the test results. More details of this validation are included in [17, 23] and hence not repeated here. Given that the number of published tests on TRC columns is limited, fire tests on CFST columns are also modelled to further validate the model, utilising the similarity between these two types of columns. A total of 23 eccentrically-loaded square, rectangular and circular CFST columns that conducted by Han et al. [43], Espinos et al. [44, 45] and Moliner et al. [46] are simulated. The details of these columns, e.g. geometric dimensions, material strengths, applied loads, load eccentricities, fire protection thicknesses and boundary conditions are listed in Table 1.

Different from TRC columns, the steel tube of a CFST column sustains the axial load directly together with the concrete core, and so loading plates are added to the ends of the CFST models to distribute the applied load to the steel tube and concrete. The loading plate is connected to the steel tube via shell-to-solid coupling. Hard contact is assumed at the interface between the concrete core and loading plate. The loading plates are modelled as rigid bodies and the axial load and boundary conditions are applied on to the corresponding reference points.

The FEA predicted fire resistance $t_{FR,p}$ is compared with the test result $t_{FR,t}$ for each test, as shown in Table 1. The average ratio between $t_{FR,p}$ and $t_{FR,t}$ is 1.07 and the standard deviation is 0.06 of all models. The FEA predicted fire resistance is on the unsafe side as compared to the test results, however, the average discrepancy between $t_{FR,p}$ and $t_{FR,t}$ is within the 10% margin, which is acceptable considering the complexity and

results variability of fire tests. The fire resistance period of the tested CFST columns in references [43-46] is mostly rather short, therefore, an insignificant difference between the predicted and measured values may lead to an apparent deviation in percentage. The differences between $t_{FR,p}$ and $t_{FR,t}$ of all CFST columns used for validation are shown in Table 1. More than 90% of these values lie within ±5 minutes and their average is only 2.1 minutes and can be generally neglected. The predicted axial deformation-time relationships of some example models are compared with the corresponding test results in Fig. 3, confirming that the developed FEA model is capable of predicting the axial deformation behaviour of eccentrically-loaded CFST columns at high temperature.

For some of the validated cases in Fig. 3 and Table 1, the discrepancy between the FEA predicted results and the corresponding test data is relatively large. This may be because: 1) The fire test results are inevitably affected by some potential uncertainties, such as the inaccuracies of the furnace-temperature control, the variabilities of the applied loading, the changes of the boundary conditions during heating and the errors in the column deformation measurement; 2) Some assumptions have been made in the FEA. For example, the published experiments [43-46] do not include measured temperature-dependant material properties of the test specimens and so these have to be assumed in the modelling. Considering the above-mentioned uncertainties, the developed FEA model could predict the axial deformation behaviour and fire resistance of eccentrically-loaded CFST columns exposed to fire relatively well. This model is used hereafter to simulate the fire performance of TRC columns under ISO 834 standard fire and eccentric load.

3. Effect of load eccentricity on the column fire behaviour

The fire performance of concentrically-loaded square and rectangular TRC columns has already been investigated by the authors in previous studies [17, 23] and the influences of key parameters, such as the load ratio, slenderness ratio and cross-sectional dimensions, on the column fire resistance have been discussed.

However, the fire behaviour of TRC columns under different load eccentricities has not yet been systematically studied. The influences of load eccentricity on the column fire performance are rather complicated, which can be divided in two folds: a) load eccentricity increases the second-order effect and causes premature failure; b) load eccentricity also leads to a reduction in the compressive force applied on to the column subject to a certain load ratio, which is actually beneficial. Depending on which of these two counteracting effects is dominant, the influence of the load eccentricity varies.

FEA modelling is carried out in this section to assess the influence of load eccentricity on the high-temperature behaviour, i.e. deformation responses, bending moments and load redistributions, of TRC columns. This then acts as the basis of the following parametric studies on the column fire resistance.

Square TRC columns are generally more used in engineering practices compared to the rectangular ones. Therefore, typical TRC columns of square sections (sectional dimension D = 600 mm, load ratio n = 0.5 and slenderness ratio λ = 30 & 50) are analysed.

For a square column, the load eccentricity ratio is defined as $2e/D$, where D is the cross-sectional width and e is the load eccentricity. The maximum load eccentricity ratio studied in this section and in the rest of this paper is 1. This is because that TRC columns are usually not designed to subject to large eccentricities since they rely on the steel tube to provide confinement to the concrete core, which is largely only effective under compression rather than bending [47].

The evolution over time of top-end axial deformation u and mid-height lateral deformation δ, obtained from FEA, is shown in Fig. 4. It should be noted that this figure shows only the deformations during heating and the deformation due to ambient-temperature loading has been deducted. All the columns investigated in Fig. 4 fail by global buckling and they experience only vertical contraction before failure. The increase in load eccentricity generally leads to the increases of axial and lateral deformations, which is particularly obvious in Figs. 4(b) and 4(d) as the load eccentricity ratio increases from 0 to 0.1.

The development over time of the mid-height bending moment of the investigated columns is shown in Fig. 5. The total bending moment M_m is the sum of the first-order moment M_e ($M_e = N_f \cdot e$) and the second-order moment M_δ ($M_\delta = N_f \cdot \delta$). The first-order moment M_e of a column subject to an arbitrary load eccentricity stays constant during heating and it is actually the initial value of total bending moment M_m. To keep the load ratio the same between all cases to allow comparison, the applied load N_f at the column top-end needs to be lowered as the load eccentricity e increases. This is because an increase in the load eccentricity results in a drop of the column's ambient-temperature buckling resistance. However, this decrease of N_f as the load eccentricity increases is not large enough to cause the first-order moment M_e to decrease, as shown in Figs. 5(b) and 5(e).

The second-order moment M_δ is due to the mid-span deformation and is shown in Figs. 5(a) and 5(d). When both the slenderness ratio and load eccentricity ratio are relatively low (e.g. $\lambda = 30$ and $2e/D \leqslant 0.1$ in Fig. 5(a)), an increase in load eccentricity generally leads to a significant increase of the second-order moment M_δ, whereas the influence of load eccentricity on M_δ becomes insignificant in the other cases.

The influence of load eccentricity on the total bending moment M_m is the superposition of the effects of eccentricity on M_e and M_δ. At a certain temperature, M_m increases as the load eccentricity increases, as shown in Figs. 5(b) and 5(e). Figs. 5(c) and 5(f) show that the proportion of second-order moment within the total moment M_δ/M_m ($M_\delta/M_m = 1/(1+e/\delta)$) increases as temperature rises, which is due to the development of the lateral deformation. At a certain temperature, this ratio M_δ/M_m decreases as the load eccentricity increases. This is because although the increase of load eccentricity e does cause the lateral deformation δ to increase, the increase rate of δ is lower than that of e, as shown in Figs. 4(b) and 4(d).

Due to the differential thermal expansion and material degradations between the steel tube, concrete core and rebars, load redistribution could occur within the composite section. The load redistribution within the mid-span cross-section of the columns

during heating is investigated.

The development during heating of the axial force ratios of concrete core, rebars and steel tube obtained from FEA are shown in Fig. 6. The axial force ratio is defined as the ratio between the axial force born by a part of the cross-section (i.e. steel tube, concrete core or rebars) and the total axial force of the cross-section. As shown in Figs. 6(a) and 6(d), although there are inevitable bond stresses and friction at the interface between the steel tube and concrete core, the axial force taken by the steel tube is negligible [17]. Therefore, the axial load applied on to a TRC section is mainly taken by the concrete core and rebars and it is redistributed between each other during heating. As temperature rises, the axial force in the concrete first decreases and then increases slightly, whereas, the axial force in the rebars increases first and then decreases due to the differential thermal expansion and differential strength degradations of these two materials [17]. Load eccentricity also affects the load distribution between the concrete and rebars. In general, an increase in the load eccentricity leads to an increase in the axial force ratio of the concrete, indicating that the applied axial load is more taken by the concrete core than by the rebars. This is mainly because the increase in load eccentricity causes the compressive stresses in the rebars in the convex side of the cross-section to decrease significantly or even turn into tension, which is discussed in detail hereafter.

Figs. 7 and 8 plot the normalized axial stress-time relationships of the concrete core and rebars of square TRC columns with slenderness ratios of 30 and 50. Compression is shown as positive in these figures. The normalized stress of concrete is given as $\sigma_{cT}/f_{c,eq,T}$, where σ_{cT} is the average axial stress across the concrete section at high temperature and $f_{c,eq,T}$ is the high-temperature equivalent compressive strength of concrete as proposed by Yang et al. [23] to consider the non-uniform temperature distribution and the influence of differential thermal stress across the cross-section. As temperature rises, σ_{cT} first decreases and then increases, which is the same as for the axial force ratio in Fig. 6, since σ_{cT} is proportional to the axial force in concrete. The high-temperature equivalent strength of concrete $f_{c,eq,T}$ decreases continually with the

increase of temperature. During the initial heating (around 7 minutes), the strength $f_{c,eq,T}$ decreases faster than the stress σ_{cT} does, and so the ratio $\sigma_{cT}/f_{c,eq,T}$ increases slightly. After this initial increase, the stress σ_{cT} becomes dominant, and so $\sigma_{cT}/f_{c,eq,T}$ decreases first then increases until failure, following the same trend as for σ_{cT} and axial force ratio, as shown in Figs. 7(a) and 8(a). As the load eccentricity ratio increases, $\sigma_{cT}/f_{c,eq,T}$ decreases, which is mainly due to the load eccentricity induced decrease of the applied load N_f. The failure stress in concrete of the concentrically-loaded column with $\lambda = 30$ reaches the equivalent compressive strength, whereas the ratios $\sigma_{cT}/f_{c,eq,T}$ of the rest of the columns remain below 0.65 during the whole heating process. This indicates the two different failure modes experienced by these columns, i.e. the relatively stocky column under concentric loading ($\lambda = 30$, $2e/D = 0$) fails by compression and the other columns experience global flexural buckling failure.

The stresses in Rebars 1 to 5 in Figs. 7 and 8, which represent all rebars utilising symmetry, are analysed. The rebar normalized stress $\sigma_{bT}/f_{b,T}$ is defined as the ratio between the axial stress σ_{bT} and the high-temperature yield strength $f_{b,T}$. For $f_{b,T}$, the tabulated values given in EC4 [25] are adopted. The rebar axial stress σ_{bT} is highly affected by the combined effects of axial compression, bending and thermal stresses due to differential thermal expansion. The rebars are of higher thermal expansion coefficient than that of the surrounding concrete, therefore, the rebars are subject to compression due to restrained thermal expansion. The compressive thermal stresses in the corner rebars are higher than those in the other rebars. For the column under concentric loading and with $\lambda = 30$, all rebars yield in compression. As the load eccentricity increases, both the first-order and second-order moments increase. For the eccentrically-loaded columns, the rebars in the concave zone (Rebar1 and Rebar2 in Figs. 7 and 8) still yield in compression, whereas the rebars in the convex zone (Rebar4 and Rebar5 in Figs. 7 and 8) experience a significant drop in compressive stresses. As shown in Figs. 7(f) and 8(f), for the columns subject to the largest eccentricity ($2e/D = 1$) analysed, the Rebar5 in the convex zone even yields in tension.

4. Ambient-temperature analysis and design

The ambient-temperature design of TRC columns is the basis of the high-temperature design. However, to the authors' knowledge, the analysis and design methods of the ambient-temperature load-bearing capacity of eccentrically-loaded rectangular TRC columns are still limited. Therefore, the ambient-temperature performance of eccentrically-loaded square and rectangular TRC columns is studied in this section, using the FEA model described in Section 2. A simplified method for the ambient-temperature buckling resistance design is then developed. The results of this section then serve as the basis of the fire performance analysis in Section 5.

The following parameters are considered: load eccentricity ratio (0 to 1), cross-sectional aspect ratio (1 to 2), bending direction (major-axis and minor-axis), cross-sectional dimension (400 to 1500 mm) and slenderness ratio (30 and 50). For a rectangular column, the load eccentricity ratio is defined as $2e/H$ if the eccentricity is applied along the direction of the sectional depth H and the eccentricity ratio is $2e/B$ where the eccentricity is applied along the direction of the sectional width B. The following properties are adopted for all the models: steel ratio α_s = 3%, reinforcement ratio ρ = 4%, concrete compressive strength f_c' = 40 MPa, steel tube yield strength f_y = 345 MPa, rebar yield strength f_b = 335 MPa, concrete cover 25 mm and pinned-pinned boundary conditions at the column ends.

4.1 Buckling resistance analysis

The Chinese standard JGJ/T471 [16] provides an indirect method for the ambient-temperature design of rectangular TRC columns and suggests to (i) convert a rectangular section of an aspect ratio no larger than 1.1 to an equivalent square section of the same area; and (ii) ignore the confinement provided by the steel tube to the concrete core, if the aspect ratio is larger than 1.1. To verify this method, the ambient-temperature load-bearing capacity of rectangular TRC columns with various sectional aspect ratios is analysed, considering both major-axis and minor-axis

bending.

The effect of cross-sectional aspect ratio on the ambient-temperature bucking resistance of TRC columns is studied in this section, as it is a key parameter characterizing rectangular cross-sections. There have been extensive studies on circular and square TRC columns, whereas limited research has been conducted on the ambient-temperature and fire performance of rectangular TRC columns. As far as the authors know, there are no specific recommendations for the sectional aspect ratios of rectangular TRC columns, and so the aspect ratios suggested by the Chinese design guide CECS 159 [48] for rectangular CFST columns are adopted. CECS 159 [48] suggests a maximum aspect ratio of 2, and so aspect ratios 1.2, 1.5, 1.8 and 2.0 are adopted in this study. To enable comparisons, the rectangular TRC columns with different sectional aspect ratios are of the same sectional area and steel ratio as those of the equivalent square section. As shown in Fig. 9, the cross-sectional areas of the rectangular columns of aspect ratios k_1 and k_2 are given by: $H_1B_1 = H_2B_2 = D^2$. Depending on the sectional aspect ratio k_i and the direction of bending, the rectangular columns are named as Rk_i-Maj and Rk_i-Min, as shown in Figs. 9(b)-9(e). When investigating the effects of aspect ratio and bending direction, the slenderness ratio remains the same for all columns.

The effects of sectional aspect ratio and load eccentricity ratio on the ambient-temperature buckling resistance of rectangular TRC columns are shown in Fig. 10. As the load eccentricity ratio increases, the column buckling resistance decreases. Fig. 10 also shows that when the aspect ratio is larger than 1.1, the buckling resistances of rectangular TRC columns are very similar to that of the equivalent square column and barely affected by the aspect ratio. To assess the degree of confinement, the buckling resistances of rectangular TRC columns are compared with their equivalent RC columns in Fig. 11(a). This figure indicates that the former is significantly larger than the latter, confirming that there is still considerable degree of confinement in rectangular TRC columns with aspect ratios larger than 1.1. As shown in Fig. 11(b), the average ratio between the buckling resistances of rectangular TRC

columns and those of their equivalent square TRC columns is 0.99. This indicates that the JGJ/T471 suggestion to ignore the confinement provided by the steel tube to the concrete core when the aspect ratio is larger than 1.1 could be over conservative. In the ambient-temperature design of rectangular TRC columns with sectional aspect ratio larger than 1.1, the confinement provided by the steel tube to the concrete core may also be considered and the rectangular section could still be converted to an equivalent square section of the same area.

4.2 Proposed design method

JGJ/T471 [16] recommends an *N*-*M* interaction diagram method for the ambient-temperature design of eccentrically-loaded square TRC columns, which is shown as follows:

$$N \le \begin{cases} \alpha_c f_{cc} A_c \beta_c r_x + (0.5 - 2/n_b) A_b f_b (r_x / 0.3 - 1.67) & 0 \le r_x \le 0.75 \\ 4(N_u - N_{r_x=0.75})(r_x - 1) + N_u & 0.75 < r_x \le 1 \end{cases} \quad (1)$$

$$M \le \begin{cases} \alpha_c f_{cc} D^3 \beta_c r_x (1 - \beta_c r_x)/2 + (M_{bf} - M_{bm})(3r_x - 1.5)^2 + M_{bm} & 0 \le r_x \le 0.75 \\ 4M_{r_x=0.75}(1 - r_x) & 0.75 < r_x \le 1 \end{cases} \quad (2)$$

where r_x is the calculation coefficient related to the cross-sectional bearing capacity of square TRC columns;

N_u is the compressive resistance under concentric loading;

A_c and A_b are the area of the concrete core and area of the rebars, respectively;

α_c is the factor to define the effective strength in the rectangular stress distribution of concrete and $\alpha_c = \begin{cases} 0.97 & f_{cu,k} \le 50 \\ 0.97 - (f_{cu,k} - 50)/1000 & 50 < f_{cu,k} \le 80 \end{cases}$;

β_c is the factor to define the effective height of the compression zone in the rectangular stress distribution of concrete and $\beta_c = \begin{cases} 0.9 & f_{cu,k} \le 50 \\ 0.9 - \left[0.16 - 0.003(80 - f_{cu,k})\right] f_{el}/f_c' & 50 < f_{cu,k} \le 80 \end{cases}$;

f_{el} is the confinement stress from the steel tube to the concrete core;

$f_{cu,k}$ is the characteristic value of the cube compressive strength of unconfined concrete;

f_{cc} is the compressive strength of confined concrete and $f_{cc} = f_c^{'} + 5.1 f_{el}$;

n_b is the number of the reinforcing bars in the cross-section;

M_{bm} is the sum of the plastic bending moment resistances of all rebars in the cross-section about the centroid of the cross-section;

M_{bf} is the sum of the plastic bending moment resistances of rebars at one edge of the cross-section about the centroid of the rebars at the opposite edge of the cross-section;

$N_{r_x=0.75}$ and $M_{r_x=0.75}$ are the compressive resistance and bending moment resistance when $r_x = 0.75$, respectively.

For the ambient-temperature design of the compressive resistance under eccentric loading N_{eu} of stocky TRC columns, N_{eu} and $N_{eu} \cdot e$ are compared directly with the *N*-*M* interaction diagram determined using Eqs. (1) and (2). As for the buckling resistance of slender columns under eccentric loading N_{eb}, the first-order bending moment $N_{eb} \cdot e$ at the column ends is modified using a coefficient η to consider the second-order effect. The maximum bending moment along the column length is given as $\eta \cdot N_{eb} \cdot e$. N_{eb} and $\eta \cdot N_{eb} \cdot e$ are then checked against the *N*-*M* interaction diagram.

The amplification coefficient η should always be equal or larger than 1.0 and it is given by,

$$\eta = \begin{cases} 1 & L_{eff}/D \le 3 \\ \dfrac{1}{800(2e/D)^{0.78}}\left(\dfrac{L_{eff}}{D}\right)^2 + 0.8 & L_{eff}/D \ge 8,\ 2e/D \le 0.3 \\ \dfrac{1}{2000(2e/D)^{1.80}}\left(\dfrac{L_{eff}}{D}\right)^2 + 0.9 & L_{eff}/D \ge 8,\ 2e/D > 0.3 \\ 1 + \left(\dfrac{L_{eff}}{5D} - \dfrac{3}{5}\right)\left(\eta_{L_{eff}/D=8} - 1\right) & 3 < L_{eff}/D < 8 \end{cases} \quad (3)$$

where L_{eff} is the effective length of the column at ambient temperature;

$\eta_{L_{eff}/D=8}$ is the value of η when $L_{eff}/D = 8$.

It should be noted that Eqs. (1) and (2) are mainly for the design of eccentrically-loaded square TRC columns according to JGJ/T471 [16] and rectangular columns of aspect ratios no larger than 1.1 are suggested to be converted into equivalent square sections. The applicability of Eqs. (1) and (2) to rectangular columns of various aspect ratios

subject to both major- and minor-axis bending is verified in this section via FEA modelling. For this verification, the following three revisions are made: 1) replacing D in Eq. (2) with $\sqrt{HB}$; 2) replacing $2e/D$ in Eq. (3) with $2e/H$ or $2e/B$; and 3) replacing L_{eff}/D in Eq. (3) with L_{eff}/H or L_{eff}/B.

Fig. 12 plots N_{eb} and $\eta \cdot N_{eb} \cdot e$ resulted from FEA modelling on the *N-M* interaction diagrams. For rectangular columns of the same sectional area, the bending moment resistance subject to pure bending increases as sectional flexural stiffness increases; their axial strengths subject to pure compression are all identical, as expected. The values of N_{eb} and $\eta \cdot N_{eb} \cdot e$ of square TRC columns and those of rectangular columns subject to major-axis bending generally lie outside the *N-M* envelope and are thus conservative. The FEA calculated N_{eb} and $\eta \cdot N_{eb} \cdot e$ of rectangular TRC columns subject to minor-axis bending usually lie within the *N-M* envelope, especially at relatively large load eccentricity, indicating the calculated *N-M* diagram is potentially unsafe for the such cases. Moreover, this *N-M* interaction diagram method is already complicated for the ambient-temperature design. Extending it to the fire design will add further complicity, which is not desirable. Therefore, a practical new method is proposed below. Eqs. (4) and (5) determine the ambient-temperature buckling resistance of square and rectangular TRC columns under eccentric loading,

$$N_{eb} = \varphi N_{eu} \tag{4}$$

$$N_{eu} = \begin{cases} \dfrac{0.45\alpha_c f_{cc} A(r_e+1)\cdot 2e/D + (r_e - 0.9\cdot 2e/D)N_u}{r_e(0.9\cdot 2e/D+1)} & 0 \le 2e/D \le 2.1r_e \\ k_4 \dfrac{k_3\alpha_c f_{cc} A(r_e+1) + (r_e - k_3 r_e - k_3)N_u}{2r_e}\left(\dfrac{1}{0.9\cdot 2e/D+1} - 0.15\right) & 2.1r_e \le 2e/D \le 5 \end{cases} \tag{5}$$

where φ is the ambient-temperature buckling reduction coefficient, which could be determined by the buckling curves given in EC3 [49] or JGJ/T471 [16];

r_e is a coefficient to divide Eq. (5) into two segmentations and $r_e = \dfrac{4M_{bm}}{\alpha_c f_{cc} D^3} + 0.5$;

A is the area of the composite section;

α_c is still the factor to define the effective strength in the rectangular stress distribution of concrete, as in Eqs. (1) and (2), however, the expression of α_c in Eq. (5) is different,

$$\alpha_c = \begin{cases} 0.81 - 0.004(f_c' - 60) & f_c' < 60 \\ 0.8 & f_c' \geq 60 \end{cases};$$

k_3 and k_4 are two factors related to r_e, $k_3 = \dfrac{1.89 r_e}{1.89 r_e + 1}$ and $k_4 = 1/(\dfrac{1}{1.89 r_e + 1} - 0.15)$.

Eq. (5) was originally proposed by Wang [50] to obtain the eccentrically-loaded compressive resistance N_{eu} of square TRC columns and it is used in this study as the basis for the determination of the eccentrically-loaded buckling resistance N_{eb}. Only the first half of Eq. (5) (for $0 \leqslant 2e/D \leqslant 2.1 r_e$) is applied in this paper, given that the investigated load eccentricity ratio is no larger than unity. Eq. (4) is to determine N_{eb}, adopting the design equation for the buckling resistance of concentrically-loaded square columns given in JGJ/T471 [16], instead of using the *N*-*M* method. When applying Eqs. (4) and (5) to rectangular columns, the following two revisions are needed: a) depending on the direction of bending, replacing $2e/D$ in Eq. (5) with $2e/H$ or $2e/B$; b) replacing r_e in Eq. (5) by $r_e = \dfrac{4M_{bm}}{\alpha_c f_{cc} (\sqrt{HB})^3} + 0.5$.

Eqs. (4) and (5) are verified against FEA modelling, as shown in Fig. 13. Various buckling curves given in EC3 [49] and JGJ/T471 [16] are adopted. For square and rectangular TRC columns, the average ratios between the calculated N_{eb} and FEA results are 1.01, 0.99, 0.96 and 0.94, when using the EC3 buckling curves (a), (b) and (c) and the JGJ/T471 curve, respectively. The corresponding standard deviations are 0.04, 0.03, 0.03 and 0.03. This demonstrates a good agreement between the proposed design method Eq. (4) and FEA, indicating the former is capable of predicting the ambient-temperature buckling resistance of eccentrically-loaded square and rectangular TRC columns. It also indicates that the choice of buckling curve has nearly no influence on the predicted results.

5. High-temperature analysis and design

Parametric studies on the fire resistance of eccentrically-loaded square and rectangular TRC columns are conducted in this section. The influences of load

eccentricity ratio (0 to 1), sectional aspect ratio (1 to 2), bending direction (major-axis and minor-axis), fire protection thickness (2 to 10 mm), sectional dimension (400 to 1500 mm), load ratio (0.4 to 0.8) and slenderness ratio (30 and 50) on the column fire resistance are investigated. In all the analysed cases, the following default parameters are adopted: moisture content 5%, steel ratio 3%, reinforcement ratio 4%, concrete compressive strength 40 MPa, steel tube yield strength 345 MPa, rebar yield strength 335 MPa, concrete cover 25 mm and pinned-pinned boundary conditions.

On the basis of the high-temperature parametric studies presented in this section, as well as the ambient-temperature design method proposed in Section 4.2, a practical fire resistance design method for square and rectangular TRC columns under eccentric loading is presented in Section 5.2.

5.1 Fire resistance analysis

The fire resistance of a TRC column is defined as the failure time at which the axial deformation or axial deformation rate reaches the limits given in ISO 834 [24]. The influence of load eccentricity ratio on the fire resistance of unprotected square columns is shown in Fig. 14. For the columns of slenderness ratio 30, the fire resistance decreases as load eccentricity ratio increases from 0 to 0.1. After the load eccentricity ratio exceeds 0.1, its negative influence on the fire resistance is insignificant. For the columns of slenderness ratio 50, the effect of load eccentricity on fire resistance is generally negligible and this is consistent with previous experimental observations [17]. In general, the load eccentricity affects the fire resistance of the columns of a relatively low slenderness (i.e. λ = 30 in Fig. 14) more than the other slenderer columns (i.e. λ = 50 in Fig. 14).

Fire protection is needed, when a column's fire resistance does not meet the required fire rating. The influence of fire protection thickness on the fire resistance of square TRC columns with various sectional dimensions, slenderness ratios, load ratios and load eccentricity ratios is investigated and shown in Fig. 15. The fire resistance of protected square TRC columns increases almost linearly with the increase in fire

protection thickness. Consistent with the behaviour of unprotected columns in Fig. 14, the influence of the load eccentricity on the column fire resistance is more significant on stockier columns than on slenderer columns.

The influence of sectional aspect ratio on the fire resistance of concentrically-loaded rectangular TRC columns that are designed to bend about the major axis was previously found to be marginal [23]. The fire performance of eccentrically-loaded rectangular TRC columns with different aspect ratios and bending directions is investigated in this research. Fig. 16 presents the relationship between the fire resistance and load eccentricity ratio for rectangular columns of various aspect ratios, subject to load eccentricities along the major and minor axes of bending. For the columns of slenderness ratio of 30, the fire resistance decreases significantly as the load eccentricity ratio increases from 0 to 0.1 and then the influence of the load eccentricity becomes insignificant. Similar to square TRC columns, the load eccentricity has a larger influence on rectangular columns of lower slenderness (λ = 30 in Fig. 16) than those of relatively large slenderness (λ = 50 in Fig. 16). The fire resistance of a rectangular column subject to a load eccentricity along the major axis is higher than that of a column, which is of the same cross-section and same slenderness ratio and under the same load ratio and same load eccentricity ratio, but subject to a load eccentricity along the minor axis. Generally, the fire resistance of Column R2.0-Maj is the highest, whereas the fire resistance of Column R2.0-Min is the lowest.

The fire performance of protected rectangular TRC columns with different load eccentricities is further analysed. The influences of load eccentricity ratio and fire protection thickness on the column fire resistance are shown in Fig. 17 as 3D scatters. For all the cases shown in Fig. 17, the fire resistance increases linearly with the increase of fire protection thickness. When the protection thickness is identical, the fire resistance of the concentrically-loaded column is generally larger than those of the eccentrically-loaded columns. The influence of aspect ratio on the column fire resistance is insignificant. The fire resistances of a pair of rectangular columns, of the

same cross-section and same slenderness ratio, under the same load ratio and same load eccentricity ratio, are not affected much by the direction of load eccentricity (i.e. major- or minor-axis).

5.2 Proposed design method

The high-temperature properties of steel tube, concrete core and rebars are determined using the simplified method proposed by Yang et al. [23]. Eqs. (4) and (5) are modified to Eqs. (6) and (7) to determine the high-temperature buckling resistance under eccentric loading $N_{eb,T}$,

$$N_{eb,T}=\varphi_T N_{eu,T} \tag{6}$$

$$N_{eu,T}=\begin{cases}\dfrac{0.45\alpha_c f_{cc,T} A(r_e+1)\cdot 2e/D+(r_e-0.9\cdot 2e/D)N_{u,T}}{r_e(0.9\cdot 2e/D+1)} & 0\le 2e/D\le 2.1r_e \\ k_4\dfrac{k_3\alpha_c f_{cc,T} A(r_e+1)+(r_e-k_3r_e-k_3)N_{u,T}}{2r_e}\left(\dfrac{1}{0.9\cdot 2e/D+1}-0.15\right) & 2.1r_e\le 2e/D\le 5\end{cases} \tag{7}$$

where $N_{eu,T}$ is the high-temperature compressive resistance under eccentric loading;

φ_T is the high-temperature buckling reduction coefficient;

$N_{u,T}$ is the high-temperature compressive resistance under concentric loading, as given by Yang et al. [23];

$f_{cc,T}$ is the high-temperature compressive strength of confined concrete and $f_{cc,T}=f_{c,eq,T}+5.1f_{el,T}$;

$f_{el,T}$ is the confinement stress from steel tube to concrete core at high temperature.

The fire resistance design of eccentrically-loaded steel-concrete composite columns is a complicated issue, as it needs to consider combined effects of heating, axial compression and bending. This paper, for the first time, develops a structural fire design method of square and rectangular TRC columns under eccentric loading. Although there are no provisions of the fire resistance design for eccentrically-loaded TRC columns in design codes worldwide, relevant methods do exist for other types of composite columns, such as CFST columns and partially encased columns. For instance, two approaches are currently available in Annexes G and H of EC4 [25] for

the fire design of eccentrically-loaded composite columns.

Annex G.7 of EC4 [25] provides a method to calculate the buckling resistance of eccentrically-loaded partially encased columns, which is valid when the eccentric load is applied inside the cross-section ($2e/D \leq 1$). This method assumes that the ratio between the buckling resistance subject to eccentric loading and that under concentric loading at high temperature is the same as that at ambient temperature, and so $N_{eb,T}$ is given as,

$$N_{eb,T}=N_{b,T}\cdot(N_{eb}/N_{b}) \tag{8}$$

where N_b and $N_{b,T}$ are the ambient-temperature and high-temperature buckling resistance under concentric loading, respectively.

Annex H.4 of EC4 [25] provides a method for the fire resistance design of eccentrically-loaded CFST columns, which uses two correction coefficients φ_s and φ_δ to modify $N_{b,T}$ into $N_{eb,T}$:

$$N_{eb,T}=N_{b,T}\cdot\varphi_s\cdot\varphi_\delta \tag{9}$$

where φ_s is a function of the percentage of reinforcement ρ; φ_δ is related to the load eccentricity ratio. φ_s and φ_δ are given in Fig. 18, in which $L_{eff,T}$ is the effective length of the column at high temperature.

As can be found from Eqs. (8) and (9), Annexes G and H of EC4 actually provide some design concepts for the high-temperature buckling resistance of CFST columns and partially encased columns, based on the relationships between $N_{eb,T}$ and $N_{b,T}$. Although the EC4 methods are not originally proposed for TRC columns, their applicability for the determination of $N_{eb,T}$ of square and rectangular TRC columns is assessed in this paper for comparison purpose. When applying Eqs. (8) and (9) given in EC4 to square and rectangular TRC columns, the detailed design equations developed by the authors in this paper and in a previous paper [23] are used for the determination of the buckling resistances N_b, $N_{b,T}$ and N_{eb}.

According to EC4 [25], the EC3 buckling curve (c) should be used to determine the reduction coefficient φ_T in the calculation methods given in Annexes G.7 and H.4. To

be consistent with the fire design method of concentrically-loaded square and rectangular TRC columns proposed earlier [23], the EC3 buckling curve (c) and the JGJ/T471 buckling curve are still recommended here to determine the reduction coefficient φ_T in Eq. (6). Figs. 19(a) and 19 (b) present the predicted buckling resistance of unprotected columns using the newly proposed method, compared with the Annex G.7 and Annex H.4 methods and the FEA modelling. For square and rectangular TRC columns, the average ratios between the calculated $N_{eb,T}$ and FEA results are 0.99, 0.96, 1.03 and 0.91, when using the proposed method with EC3 buckling curve (c), proposed method with JGJ/T471 buckling curve, Annex G.7 method and Annex H.4 method, respectively. The corresponding standard deviations are 0.07, 0.07, 0.08 and 0.08.

The proposed method gives the closest predictions to the FEA results, confirming that this method is appropriate for the determination of the buckling resistance under eccentric loading of square and rectangular TRC columns exposed to fire. The Annex H.4 and Annex G.7 methods present slightly worse comparisons against the FEA results. That is probably because some of the parameters adopted here are beyond the applicability of these two methods, however, this should not affect the general applicability of these two methods on TRC columns.

The above-proposed method for unprotected TRC columns is further extended to protected columns. The simplified equations proposed previously [23] for the determination of the temperature profile of protected TRC columns are adopted. The comparison between the predicted buckling resistance of protected columns and the FEA modelling is shown in Figs. 19(c) and 19(d). The EC3 buckling curve (c) and the JGJ/T471 buckling curve are still used to determine the high-temperature buckling reduction coefficient φ_T. For protected TRC columns, the average ratios between the calculated $N_{eb,T}$ and FEA results are 0.99 and 0.96, when using the proposed method with EC3 buckling curve (c) and JGJ/T471 buckling curve, respectively. The corresponding standard deviations are 0.08 and 0.08. These good agreements between the predicted and FEA results indicate that the proposed method is capable of

determining the fire resistance of protected square and rectangular TRC columns under eccentric loading.

To sum up, a practical design method is proposed in this paper for the ambient-temperature and high-temperature design of eccentrically-loaded square and rectangular TRC columns with and without fire protection. For rectangular TRC columns, this method is applicable to those of sectional aspect ratios no larger than 2.

6. Conclusions

Based on a well-validated sequentially-coupled thermo-mechanical FEA model, 2912 numerical simulations considering various parameters have been conducted to investigate the fire performance of eccentrically-loaded square and rectangular TRC columns. The following conclusions could be drawn within the research scope of this paper:

(1) The influences of cross-sectional aspect ratio and bending direction on the ambient-temperature buckling resistance of eccentrically-loaded rectangular columns are insignificant, for columns of the same cross-sectional area and of the same slenderness ratio. Therefore, rectangular columns of sectional aspect ratios no larger than 2 could be converted into equivalent square sections in the design;

(2) Most of the eccentrically-loaded square TRC columns analysed experience only axial contraction during heating and fail by deformation runaway. The axial load applied to a TRC column is mainly sustained by the inner RC section and it is firstly transferred from the concrete core to the rebars and then redistributed back to the concrete;

(3) Load eccentricity has a greater influence on columns of relatively low slenderness than those of relatively high slenderness. The fire resistances of rectangular columns subject to major-axis bending are generally larger than those of the same cross section and the same slenderness, under the same load ratio, but subject to minor-axis bending. The fire resistance of a protected TRC column increases almost linearly with the increase in the fire protection thickness;

(4) A practical method is proposed for the fire resistance design of eccentrically-loaded square and rectangular TRC columns of sectional aspect ratios no larger than 2, with and without protection. This method has been validated well

against FEA. The EC3 buckling curve (c) and JGJ/T471 buckling curve are recommended for the determination of high-temperature buckling reduction coefficients.

Acknowledgements

The authors gratefully acknowledge the National Natural Science Foundation of China (51878220) for the financial support.

Reference

[1] S.M. Zhang, J.P. Liu, Seismic behavior and strength of square tube confined reinforced-concrete (STRC) columns, J. Constr. Steel Res. 63 (2007) 1194–1207.

[2] J.P. Liu, S.M. Zhang, X.D. Wang, L.H. Guo, Behavior and strength of circular tube confined reinforced-concrete (CTRC) columns, J. Constr. Steel Res. 65 (2009) 1447–1458.

[3] J.P. Liu, X.D. Wang, S.M. Zhang, Behavior of square tubed reinforced-concrete short columns subjected to eccentric compression, Thin-Walled Struct. 91 (2015) 108–115.

[4] M. Tomii, K. Sakino, K. Watanabe, Y. Xiao, Lateral Load Capacity of Reinforced Concrete Short Columns Confined by Steel Tube, Proceedings of the International Speciality Conference on Concrete Filled Steel Tubular Structures, Harbin, China (1985), 19–26.

[5] M. Tomii, K. Sakino, Y. Xiao, K, Watanabe, Earthquake Resisting Hysteretic Behavior of Reinforced Concrete Short Columns Confined by Steel Tube, Proceedings of the International Speciality Conference on Concrete Filled Steel Tubular Structures, Harbin, China (1985), 119–125.

[6] M.J.N. Priestley, F. Seible, Y. Xiao, R. Verma, Steel jacket retrofitting of reinforced concrete bridge columns for enhanced shear strength-part 1：theoretical considerations and test design, ACI Struc. J. 91 (4) (1994) 394–405.

[7] Y.P. Sun, K. Sakino, Earthquake-resisting performance of RC columns confined by

square steel tube, Part 3: effects of shear span ratio of column, J. Struct. Constr. Eng. AIJ. 547 (2001) 129–136.

[8] R.S. Aboutaha, R. Machado, Seismic resistance of steel confined reinforced concrete (SCRC) columns, Struct. Des. Tall Buil. 7 (3) (1998) 251–260.

[9] L.H. Han, G.H. Yao, Z.B. Chen, Q. Yu, Experimental behaviours of steel tube confined concrete (STCC) columns, Steel Compos. Struct. 5 (6) (2005) 459–484.

[10] L.H. Han, H. Qu, Z. Tao, Z.F. Wang, Experimental behaviour of thin-walled steel tube confined concrete column to RC beam joints under cyclic loading, Thin-Walled Struct. 47 (8-9) (2009) 847–857.

[11] Q. Yu, Z. Tao, W. Liu, Z.B. Chen, Analysis and calculations of steel tube confined concrete (STCC) stub columns, J. Constr. Steel Res. 66 (1) (2010) 53–64.

[12] J.A. Abdullah, S.M. Zhang, J.P. Liu, Shear strength and behavior of tubed reinforced and steel reinforced concrete (TRC and TSRC) short columns, Thin-Walled Struct. 48 (3) (2010) 191–199.

[13] X.H. Zhou, J.P. Liu, Seismic behavior and shear strength of tubed RC short columns, J. Constr. Steel Res. 66 (3) (2010) 385–397.

[14] X.D. Wang, J.P. Liu, S.M. Zhang, Behavior of short circular tubed-reinforced-concrete columns subjected to eccentric compression, Eng. Struct. 105 (2015) 77–86.

[15] X.H. Zhou, J.P. Liu, X.D. Wang, Y.F. Chen, Behavior and design of slender circular tubed-reinforced-concrete columns subjected to eccentric compression, Eng. Struct. 124 (2016) 17–28.

[16] JGJ/T471, Technical Standard for Steel Tube Confined Concrete Structures, MOHURD (Ministry of Housing and Urban-Rural Development of the People's Republic of China), Beijing, China, 2020 [In Chinese]

[17] D.D. Yang, F.Q. Liu, S.S. Huang, H. Yang, ISO 834 standard fire test and mechanism analysis of square tubed-reinforced-concrete columns, J. Constr. Steel Res. 175 (2020), 106316.

[18] F.Q. Liu, L. Gardner, H. Yang, Post-fire behaviour of reinforced concrete stub

columns confined by circular steel tubes, J. Constr. Steel Res. 102 (2014) 82–103.

[19] F.Q. Liu, H. Yang, L. Gardner, Post-fire behaviour of eccentrically loaded reinforced concrete columns confined by circular tubes, J. Constr. Steel Res. 122 (2016) 495–510.

[20] F.Q. Liu, Y.Y. Wang, L. Gardner, A.H. Varma, Experimental and numerical studies of reinforced concrete columns confined by circular steel tubes exposed to fire, J. Struct. Eng. 145 (2019) 04019130.

[21] F.Q. Liu, H. Yang, R. Yan, W. Wang, Experimental and numerical study on behaviour of square steel tube confined reinforced concrete stub columns after fire exposure, Thin-Walled Struct. 139 (2019) 105–125.

[22] F.Q. Liu, H. Yang, W. Wang, Behaviours of concentrically and eccentrically loaded square steel tube confined reinforced concrete slender columns after fire exposure, Thin-Walled Struct. 158 (2021) 107155

[23] D.D. Yang, F.Q. Liu, S.S. Huang, H. Yang, Structural fire safety design of square and rectangular tubed-reinforced-concrete columns, Structures. 29 (2021) 1286–1321.

[24] ISO 834-1, Fire Resistance Test-Elements of Building Construction, Part 1: General Requirements, International Organization for Standardization ISO 834, Geneva, Switzerland, 1999.

[25] EN 1994-1-2, Eurocode 4 - Design of Composite Steel and Concrete Structures - Part 1-2: General Rules - Structural Fire Design, CEN, Brussels, 2008.

[26] T.T. Lie, Fire resistance of circular steel columns filled with bar-reinforced concrete, J. Struct. Eng. 120 (1994) 1489–1509.

[27] L.H. Han. Concrete Filled Steel Tubular Structures-Theory and Practice (third edition), Science Press, Beijing (China) (2016) [in Chinese]

[28] J. Ding, Y.C. Wang, Realistic modelling of thermal and structural behaviour of unprotected concrete filled tubular columns in fire, J. Constr. Steel Res. 64 (2008) 1086–1102.

[29] GB 51249-2017, Code for fire safety of steel structures in buildings, MOHURD

(Ministry of Housing and Urban-Rural Development of the People's Republic of China), Beijing, China, 2018 [In Chinese]

[30] L.H. Han, X.L. Zhao, Y.F. Yang, J.B. Feng, Experimental study and calculation of fire resistance of concrete-filled hollow steel columns, J. Struct. Eng. 129 (3) (2003) 346–356.

[31] Xiong MX, Fire resistance of ultra-high strength concrete filled steel tubular columns. Doctoral dissertation, Singapore: National University of Singapore, 2013.

[32] W.Y. Wang, G.Q. Li, Fire-resistance study of restrained steel columns with partial damage to fire protection, Fire Saf. J. 44 (8) (2009)1088–1094.

[33] G.Q. Li, W.Y. Wang, S.W. Chen, A simple approach for modeling fire-resistance of steel columns with locally damaged fire protection, Eng. Struct. 31(3) (2009) 617–622.

[34] P.F. Ren, X.M. Hou, Q. Rong, W.Z. Zheng, Quantifying fire insulation effects on the fire response of hybrid-fiber reinforced reactive powder concrete beams, Fire Technol. 56 (9) (2020) 1487–1525.

[35] M.M.S. Dwaikat, V.K.R. Kodur, A simplified approach for predicting temperatures in fire exposed steel members, Fire Saf. J. 55 (1) (2013) 87–96.

[36] V.K.R. Kodur, B. Yu, R. Solhmirzaei, A simplified approach for predicting temperatures in insulated RC members exposed to standard fire, Fire Saf. J. 92 (2017) 80–90.

[37] A.H. Buchanan, A.K. Abu, Structural design for fire safety, John Wiley & Sons, New Zealand (2017) 124–126.

[38] J.A. Purkiss, Fire Safety Engineering Design of Structures, second ed., Butter-worth-Heinemann, Linacre House, Jordan Hill, Oxford OX2 8DP, UK, 2007.

[39] U. Wickstrom, E. Hadziselimovic, Equivalent concrete layer thickness of a fire protection insulation layer, Fire Saf. J. 26 (1996) 295–302.

[40] GB 50936, Technical Code for Concrete Filled Steel Tubular Structures,

MOHURD (Ministry of Housing and Urban-Rural Development of the People's Republic of China), Beijing, China, 2014 [In Chinese]

[41] S. Hong, A.H. Varma, Analytical modeling of the standard fire behavior of loaded CFT columns, J. Constr. Steel Res. 65 (2009) 54–69.

[42] A. Espinos, M.L. Romero, A. Hospitaler, Advanced model for predicting the fire response of concrete filled tubular columns, J. Constr. Steel Res. 66 (2010) 1030–1046.

[43] L.H. Han, Y.F. Yang, L. Xu, An experimental study and calculation on the fire resistance of concrete-filled SHS and RHS columns, J. Constr. Steel Res. 59 (2003) 427–452.

[44] A. Espinos, M.L. Romero, E. Serra, A. Hospitaler, Circular and square slender concrete-filled tubular columns under large eccentricities and fire, J. Constr. Steel Res. 110 (2015) 90–100.

[45] A. Espinos, M.L. Romero, E. Serra, A. Hospitaler, Experimental investigation on the fire behaviour of rectangular and elliptical slender concrete-filled tubular columns, Thin-Walled Struct. 93 (2015) 137–148.

[46] V. Moliner, A. Espinos, M.L. Romero, A. Hospitaler, Fire behavior of eccentrically loaded slender high strength concrete-filled tubular columns, J. Constr. Steel Res. 83 (2013) 137–146.

[47] H. Yang, F.Q. Liu, L. Gardner, Post-fire behaviour of slender reinforced concrete columns confined by circular steel tubes, Thin-Walled Struct. 87 (2015) 12–29.

[48] CECS 159, Technical Specification for Structures with Concrete-filled Rectangular Steel Tube Members, CECS (China Association for Engineering Construction Standardization), Beijing, China, 2004 [In Chinese]

[49] EN 1993-1-1, Eurocode 3 - Design of Steel Structures - Part 1-1: General Rules and Rules for Buildings, CEN, Brussels, 2005.

[50] Wang XD, Study on the behavior and strength of TRC and TSRC columns. Doctoral dissertation, Harbin, China : Harbin Institute of Technology, 2017 19–20. [In Chinese]

Nomenclature

N_u	Ambient-temperature compressive resistance under concentric loading
N_b	Ambient-temperature buckling resistance under concentric loading
N_{eu}	Ambient-temperature compressive resistance under eccentric loading
N_{eb}	Ambient-temperature buckling resistance under eccentric loading
$N_{u,T}$	High-temperature compressive resistance under concentric loading
$N_{b,T}$	High-temperature buckling resistance under concentric loading
$N_{eu,T}$	High-temperature compressive resistance under eccentric loading
$N_{eb,T}$	High-temperature buckling resistance under eccentric loading
N_f	Applied load in fire
M_m	Total bending moment
M_e	First-order bending moment
M_δ	Second-order bending moment
φ	Ambient-temperature buckling reduction coefficient
φ_T	High-temperature buckling reduction coefficient
n	Load ratio
λ	Slenderness ratio
$t_{FR,t}$	Tested fire resistance
$t_{FR,p}$	Predicted fire resistance
A	Cross-sectional area of the composite section
A_c	Cross-sectional area of the concrete core
A_b	Cross-sectional area of the rebars
D	Cross-sectional dimension of a square section
H	Cross-sectional depth of a rectangular section
B	Cross-sectional width of a rectangular section
k	Cross-sectional aspect ratio
t_s	Steel tube thickness
d_p	Fire protection thickness

u	Axial deformation
δ	Lateral deformation
e	Load eccentricity
$2e/D$	Load eccentricity ratio of a square section
$2e/H$	Load eccentricity ratio of a rectangular section along the major axis
$2e/B$	Load eccentricity ratio of a rectangular section along the minor axis
ϕ	Diameter of a reinforcing bar
L	Whole length of a column
L_{eff}	Effective length of a column at ambient temperature
$L_{\mathrm{eff},T}$	Effective length of a column at high temperature
σ_{cT}	Average axial stress of the whole concrete section at high temperature
f_{cc}	Compressive strength of confined concrete at ambient temperature
f_{c}'	Compressive strength of unconfined concrete at ambient temperature
$f_{\mathrm{cu,k}}$	Characteristic value of the cube compressive strength of concrete
$f_{\mathrm{c,eq},T}$	High-temperature equivalent compressive strength of unconfined concrete
σ_{bT}	Axial stress of the rebar at high temperature
f_{b}	Ambient-temperature yield strength of the rebar
$f_{\mathrm{b},T}$	High-temperature yield strength of the rebar
f_{y}	Ambient-temperature yield strength of the steel tube
f_{el}	Confinement stress from steel tube to concrete core at ambient temperature
$f_{\mathrm{cc},T}$	Compressive strength of confined concrete at high temperature
$f_{\mathrm{el},T}$	Confinement stress from steel tube to concrete core at high temperature
φ_{s}	A coefficient related to reinforcement ratio
φ_{δ}	A coefficient related to load eccentricity ratio

Figures and Tables

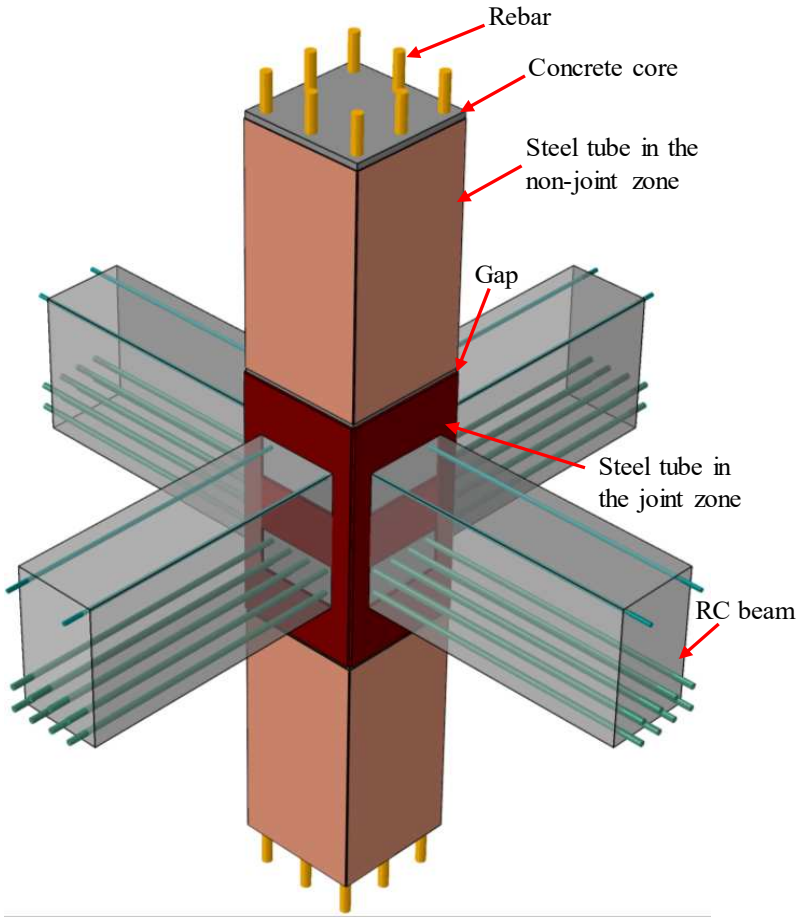

Fig. 1. Schematics of TRC column and TRC column-RC beam connection

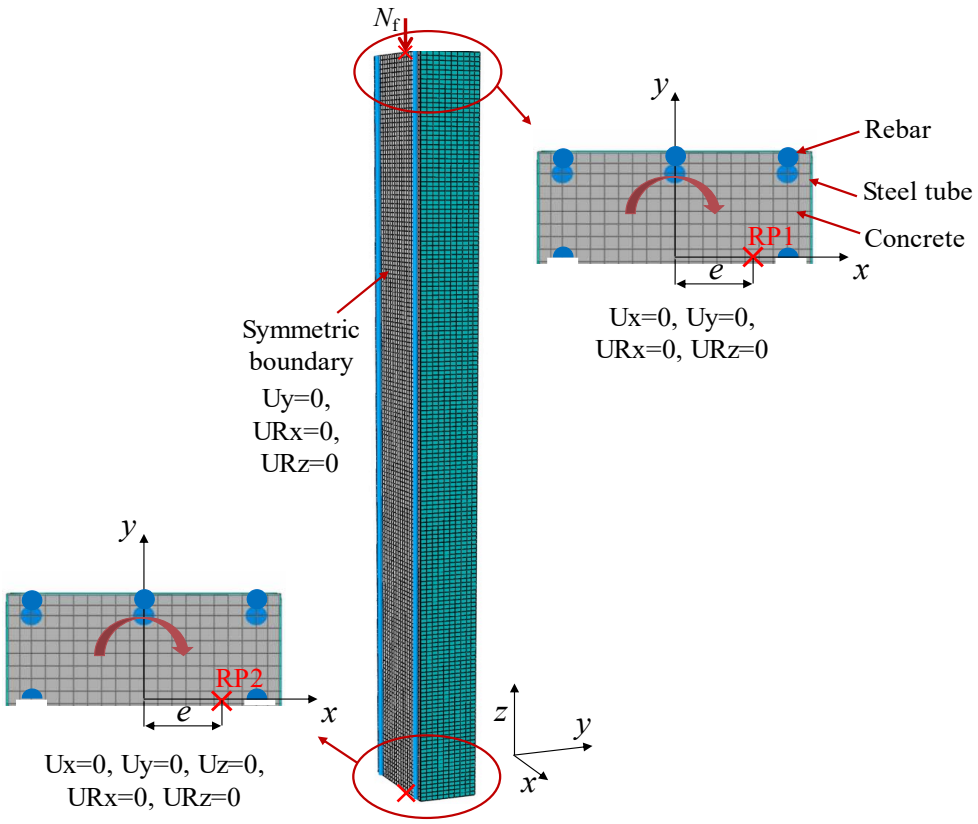

Fig. 2. Illustration of the mechanical FEA model

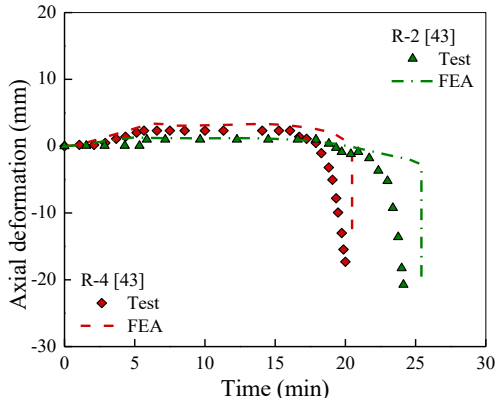

(a) R-2 & R-4

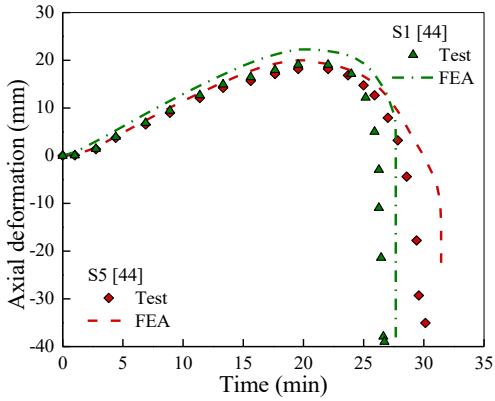

(b) S1 & S5

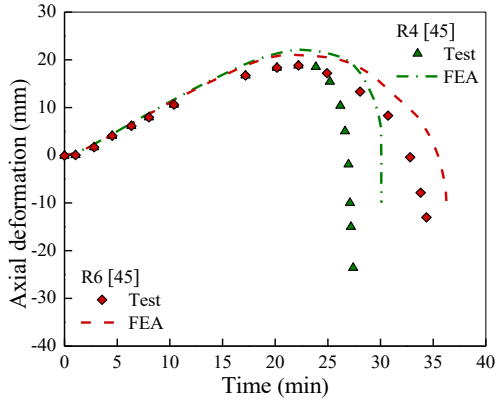

(c) R4 & R6

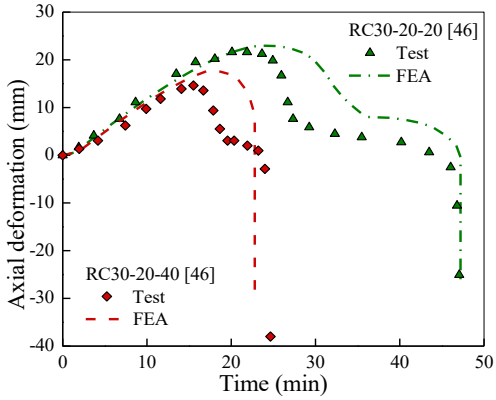

(d) RC30-20-20 & RC30-20-40

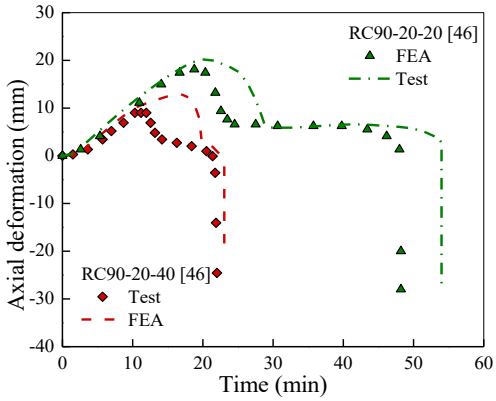

(e) RC90-20-20 & RC90-20-40

Fig. 3. Axial deformation-time curves given by FEA vs test results on CFST columns.

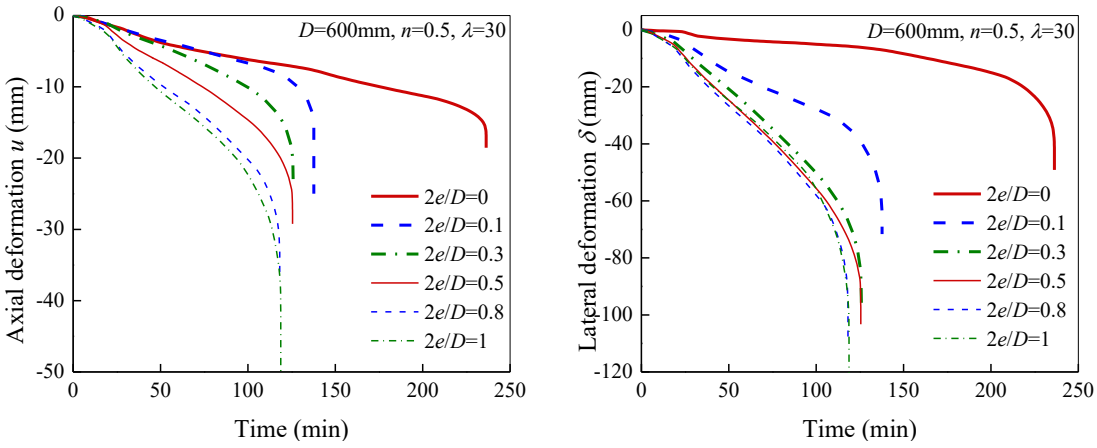

(a) Axial deformation (λ=30) (b) Lateral deformation (λ=30)

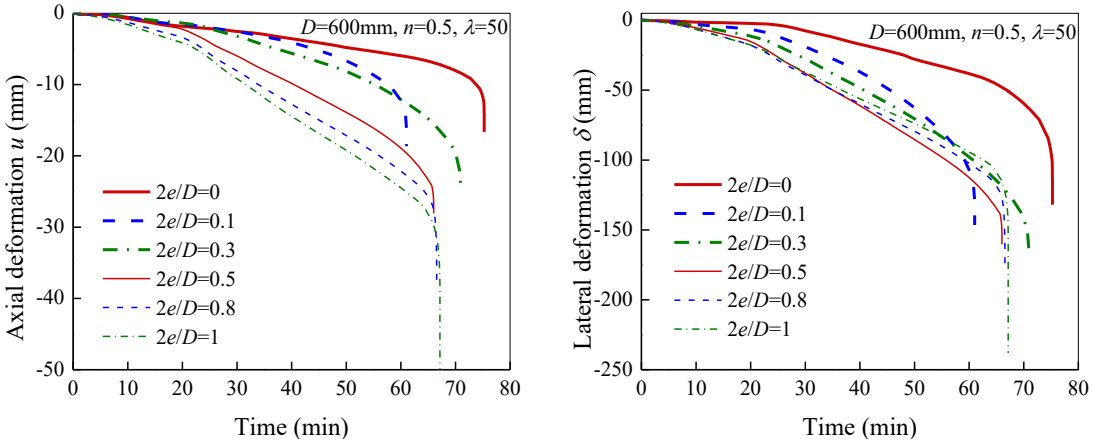

(c) Axial deformation (λ=50) (d) Lateral deformation (λ=50)

Fig. 4. Influence of load eccentricity ratio on the overall deformations of square TRC columns
(D=600 mm, n=0.5).

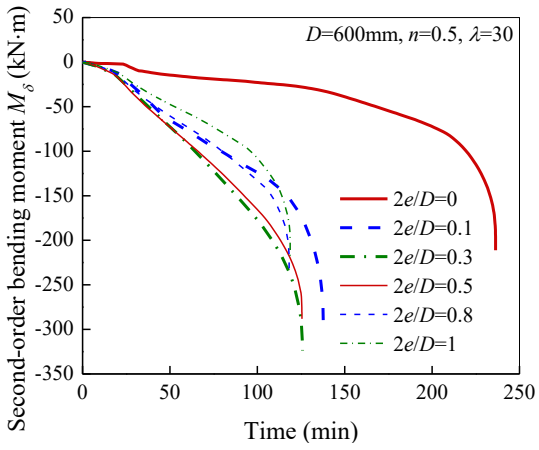

(a) Second-order bending moment (λ=30)

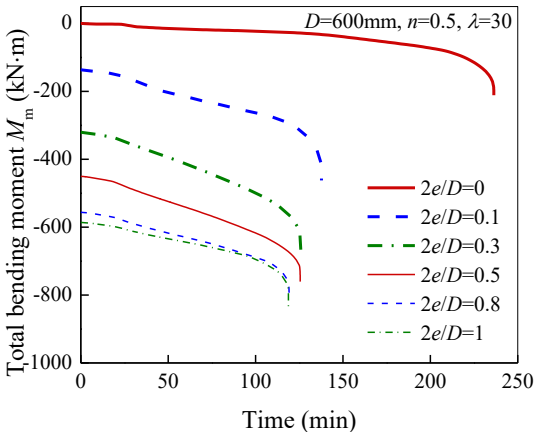

(b) Total bending moment (λ=30)

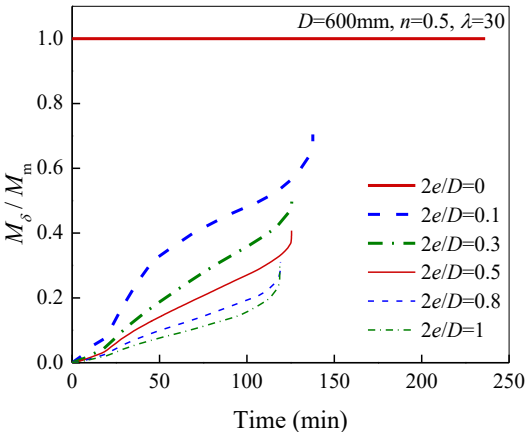

(c) Percentage of second-order moment (λ=30)

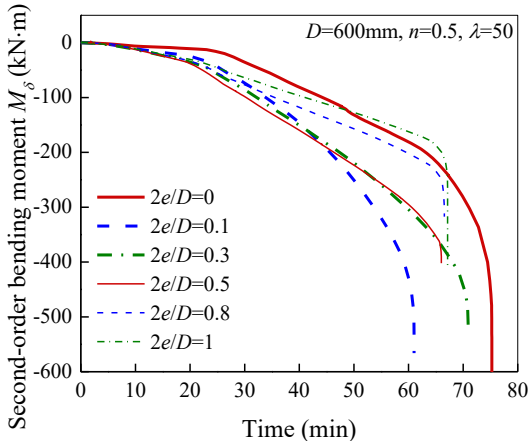

(d) Second-order bending moment (λ=50)

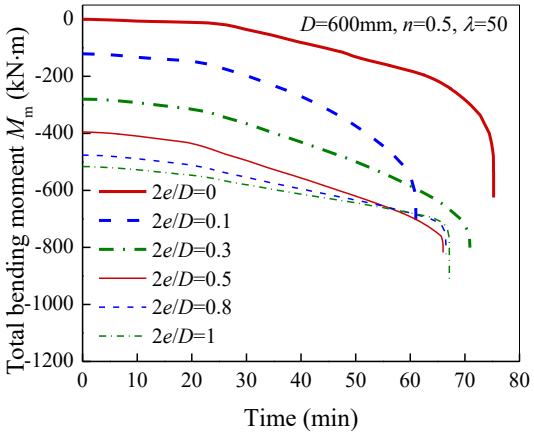

(e) Total bending moment (λ=50)

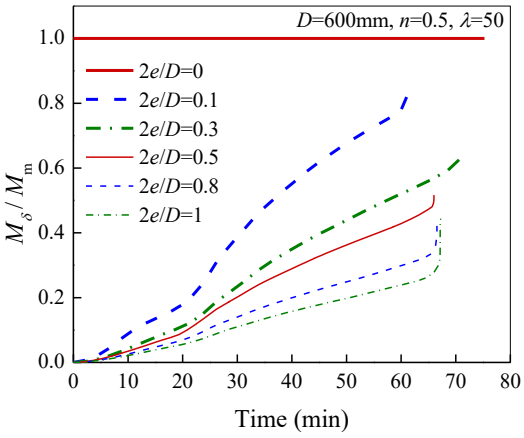

(f) Percentage of second-order moment (λ=50)

Fig. 5. Influence of load eccentricity ratio on the bending moments of square TRC columns (D=600 mm, n=0.5).

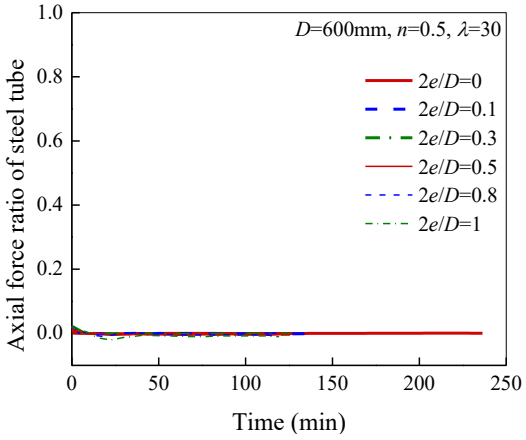

(a) Axial force ratio of steel tube (λ=30)

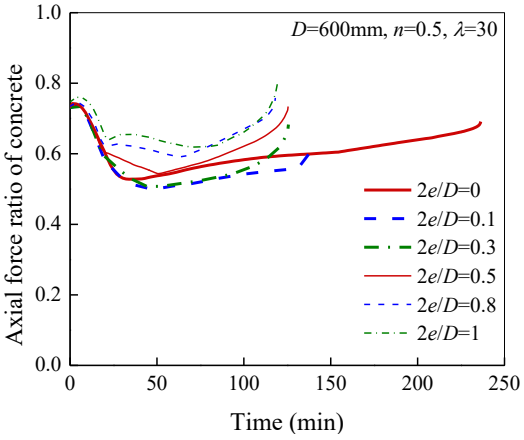

(b) Axial force ratio of concrete (λ=30)

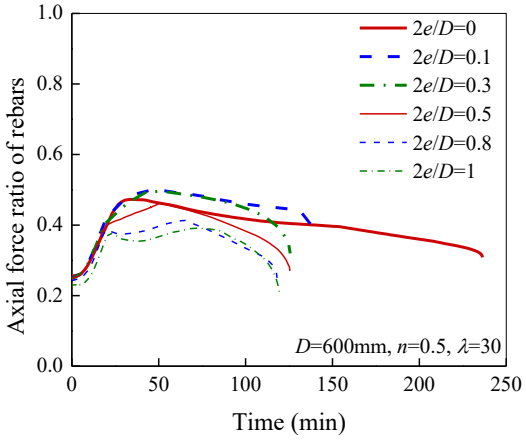

(c) Axial force ratio of rebars (λ=30)

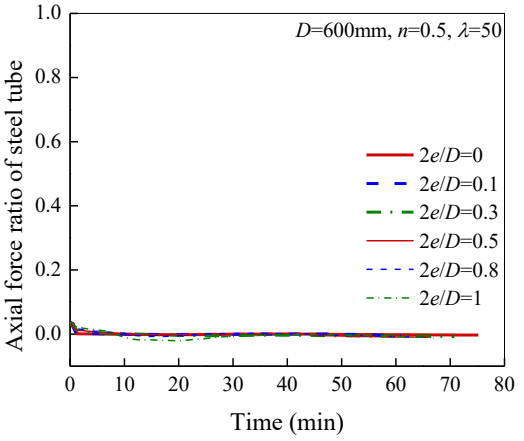

(d) Axial force ratio of steel tube (λ=50)

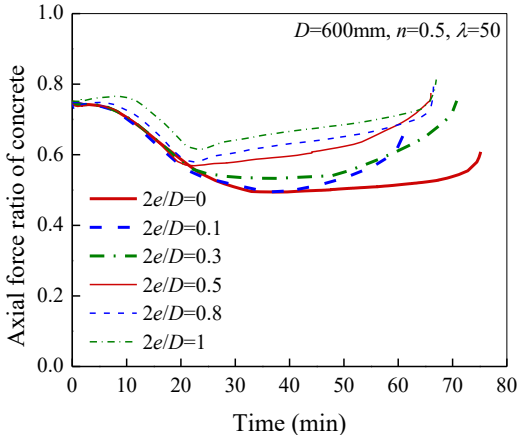

(e) Axial force ratio of concrete (λ=50)

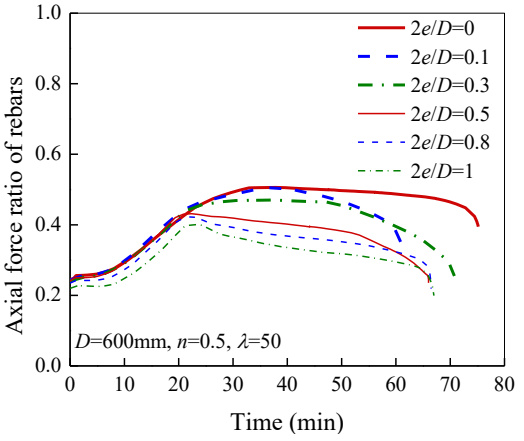

(f) Axial force ratio of rebars (λ=50)

Fig. 6. Influence of load eccentricity ratio on the load redistributions of square TRC columns (D=600 mm, n=0.5).

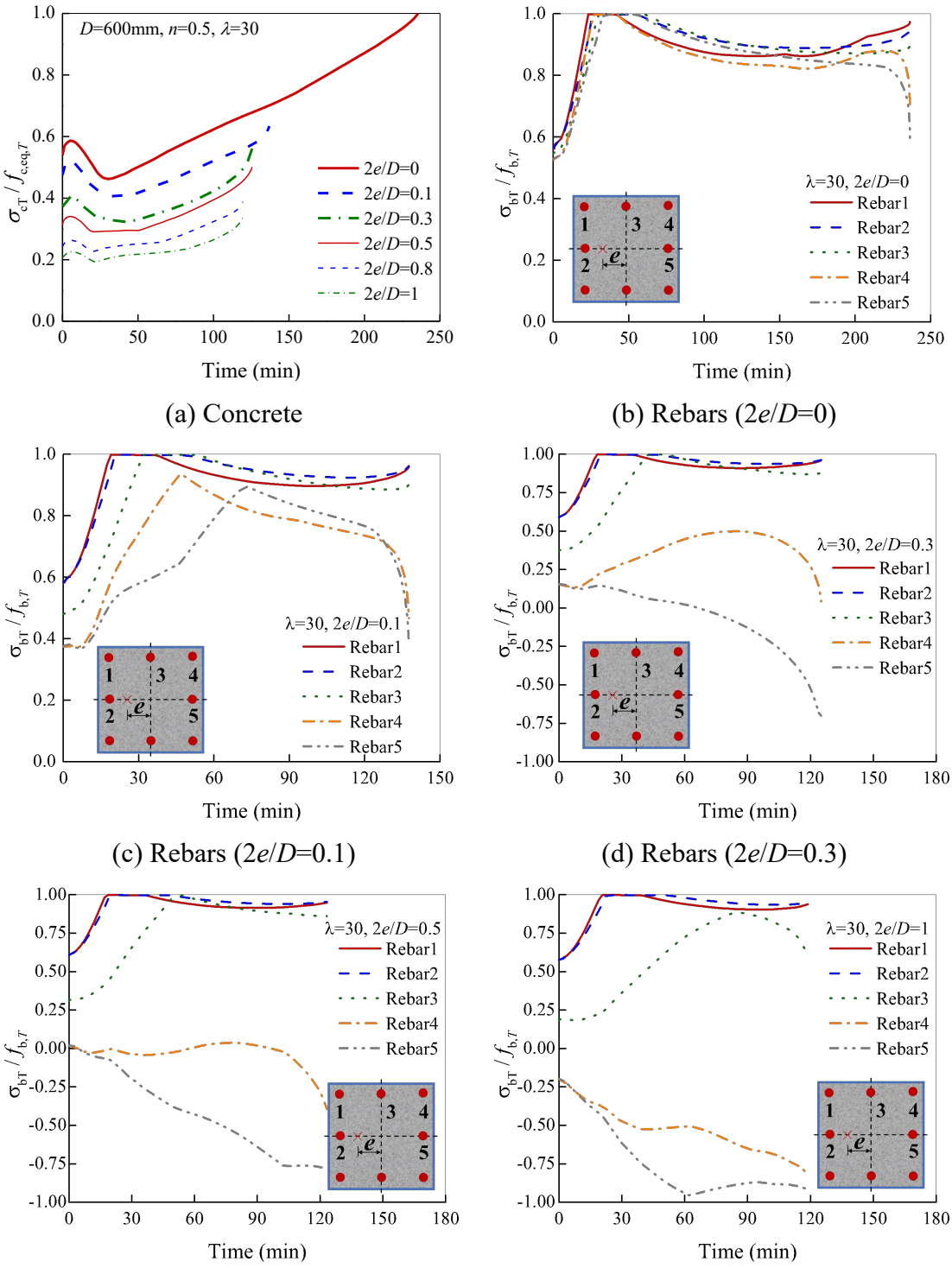

(a) Concrete

(b) Rebars (2*e*/*D*=0)

(c) Rebars (2*e*/*D*=0.1)

(d) Rebars (2*e*/*D*=0.3)

(e) Rebars (2*e*/*D*=0.5)

(f) Rebars (2*e*/*D*=1)

Fig. 7. Normalized axial stress-time curves of the concrete core and rebars of square TRC columns with *D*=600 mm, *n*=0.5, *λ*=30.

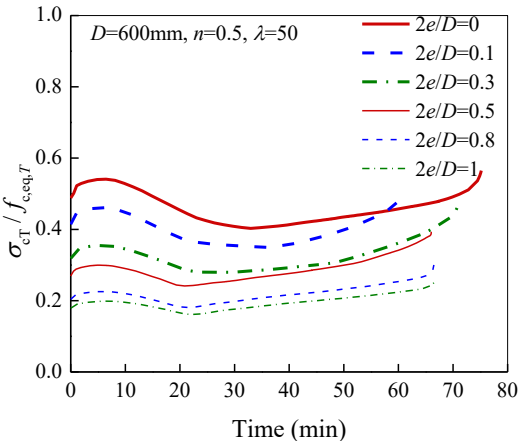

(a) Concrete

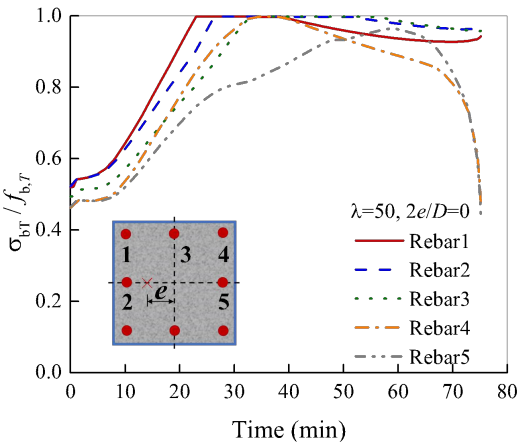

(b) Rebars (2*e*/*D*=0)

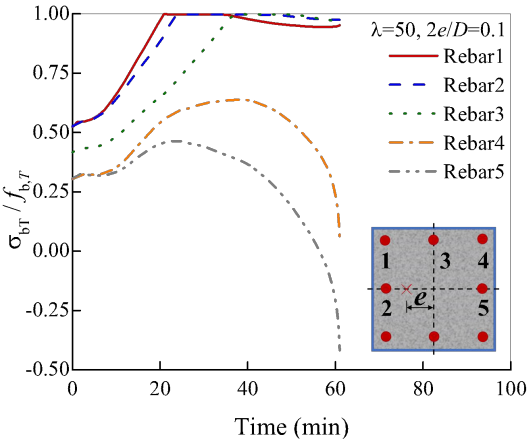

(c) Rebars (2*e*/*D*=0.1)

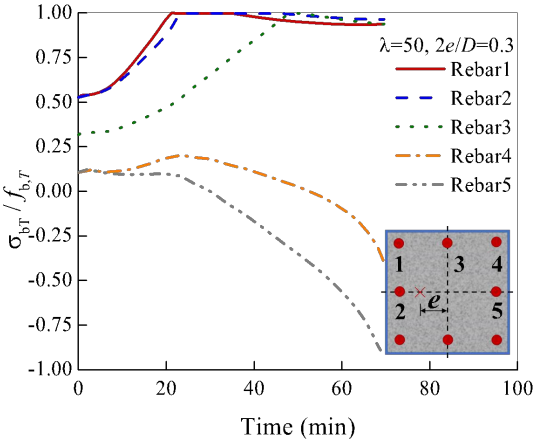

(d) Rebars (2*e*/*D*=0.3)

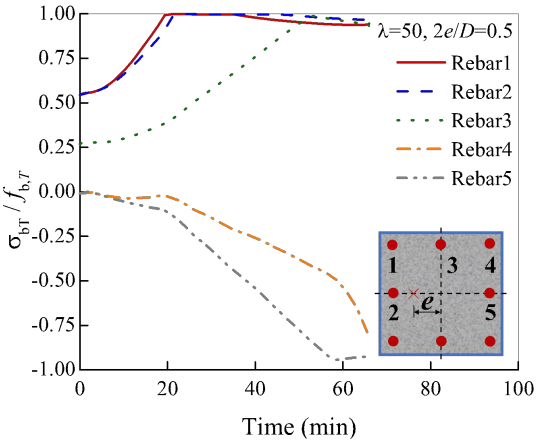

(e) Rebars (2*e*/*D*=0.5)

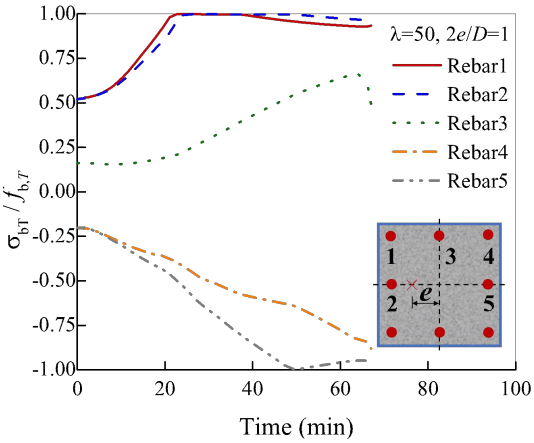

(f) Rebars (2*e*/*D*=1)

Fig. 8. Normalized axial stress-time curves of the concrete core and rebars of square TRC columns with *D*=600 mm, *n*=0.5, *λ*=50.

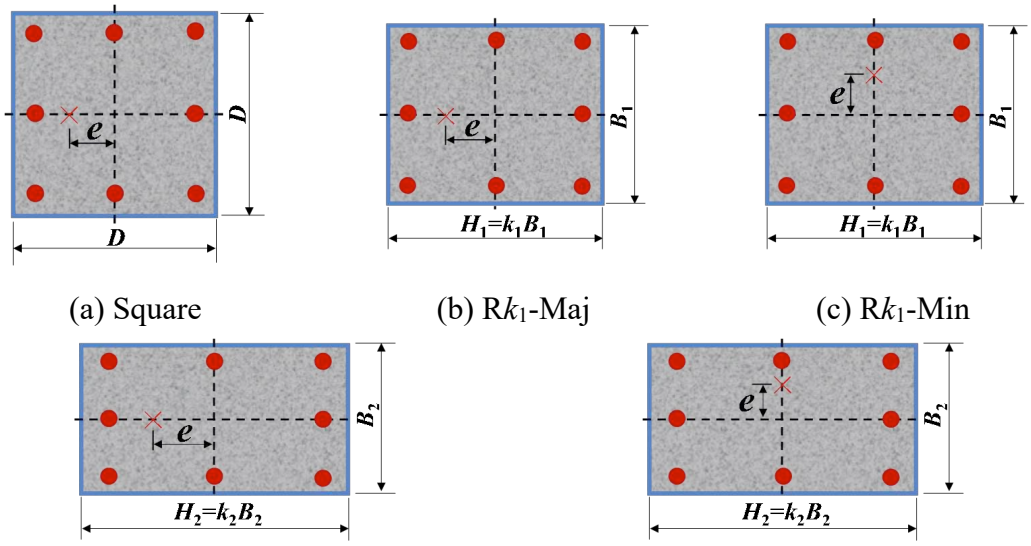

(a) Square (b) Rk_1-Maj (c) Rk_1-Min

(d) Rk_2-Maj (e) Rk_2-Min

Fig. 9. Rectangular sections with different sectional aspect ratios and bending directions and the equivalent square section.

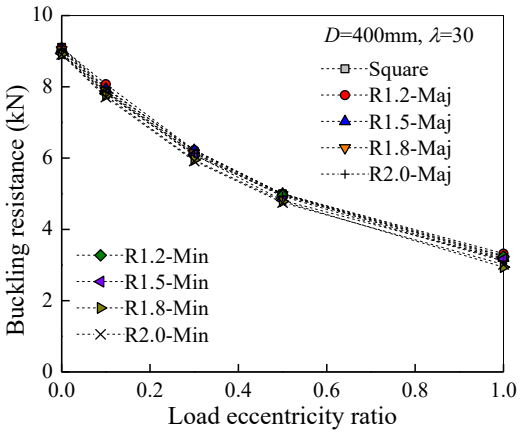

(a) D=400 mm, λ=30

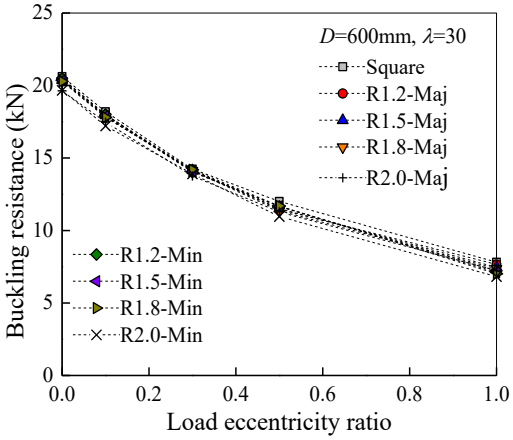

(b) D=600 mm, λ=30

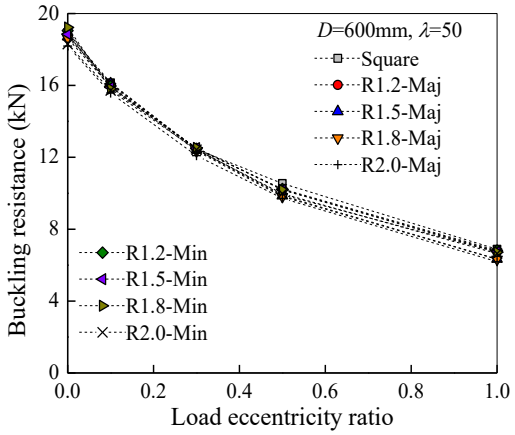

(c) D=600 mm, λ=50

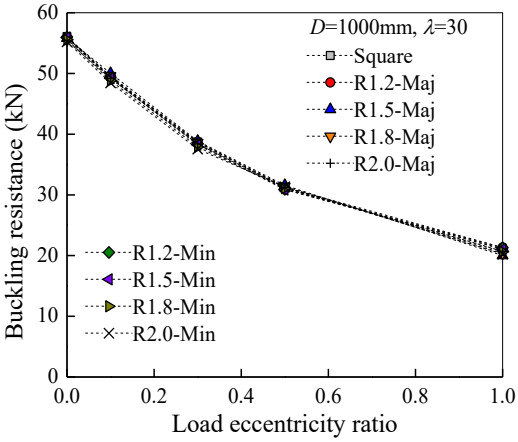

(d) D=1000 mm, λ=30

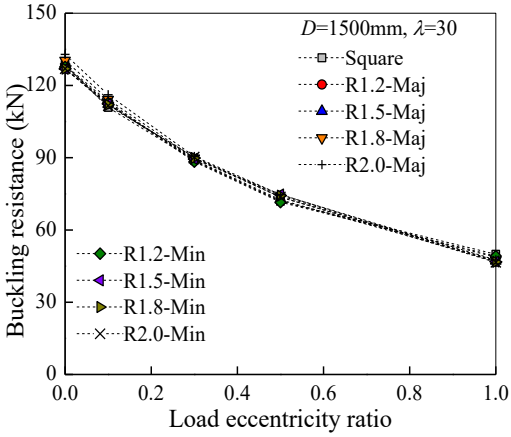

(e) D=1500 mm, λ=30

Fig. 10. Influences of aspect ratio and load eccentricity ratio on the ambient-temperature buckling resistance of rectangular TRC columns.

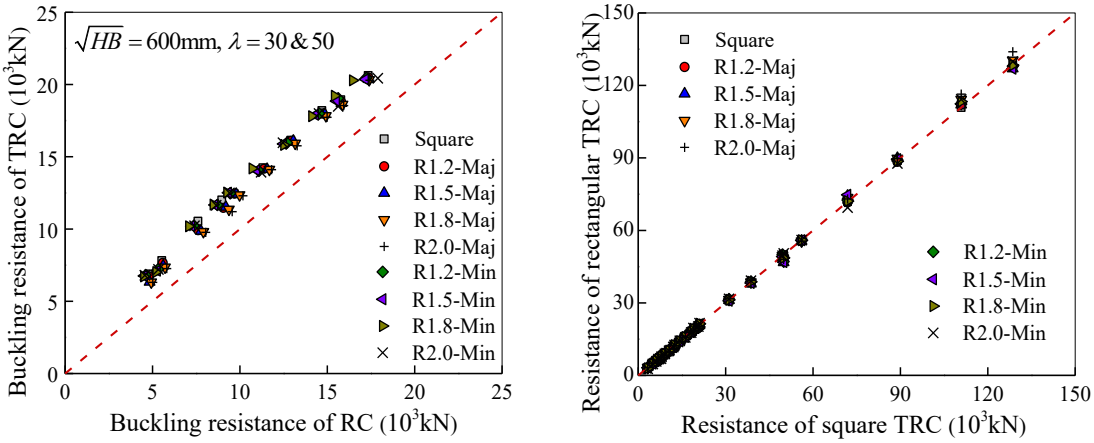

(a) RC columns (D=600 mm, λ=30 & 50) (b) Equivalent square TRC columns

Fig. 11. Comparison between the buckling resistance of rectangular TRC columns and RC columns & equivalent square TRC columns.

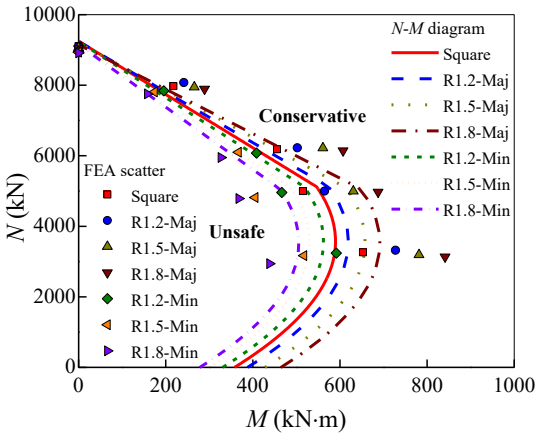

(a) D=400 mm, λ=30

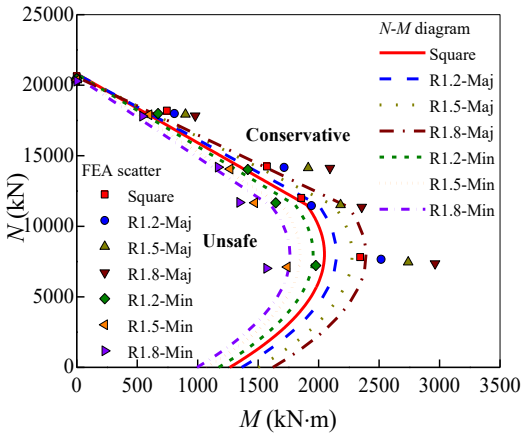

(b) D=600 mm, λ=30

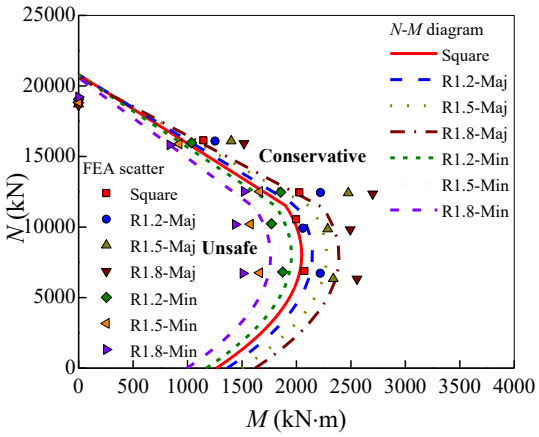

(c) D=600 mm, λ=50

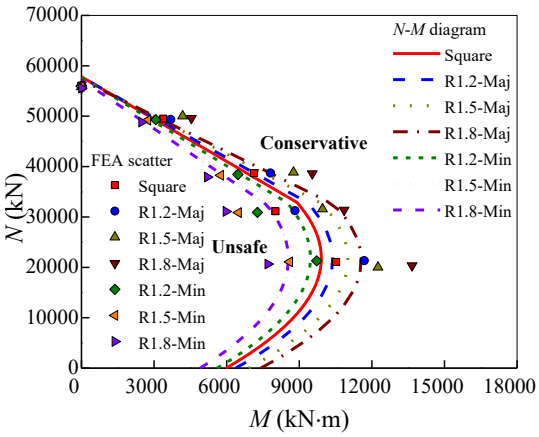

(d) D=1000 mm, λ=30

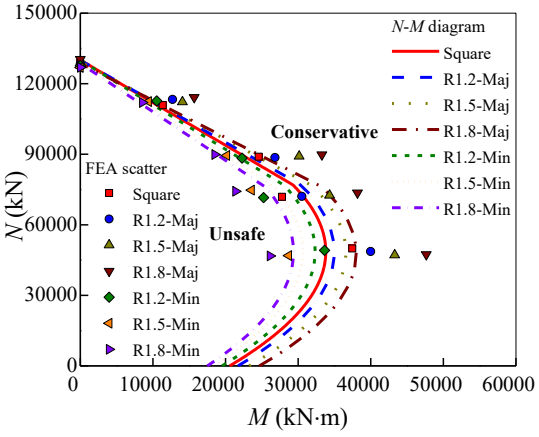

(e) D=1500 mm, λ=30

Fig. 12. Comparison between the predicted ambient-temperature buckling resistance under eccentric loading using the *N-M* interaction diagram method and FEA results.

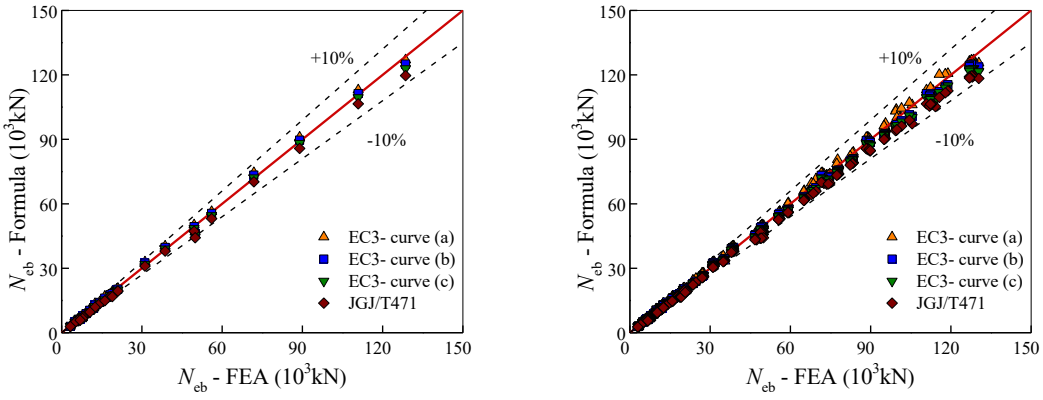

(a) Square TRC (b) Rectangular TRC

Fig. 13. Comparison between the predicted ambient-temperature buckling resistance under eccentric loading using the proposed method and FEA results.

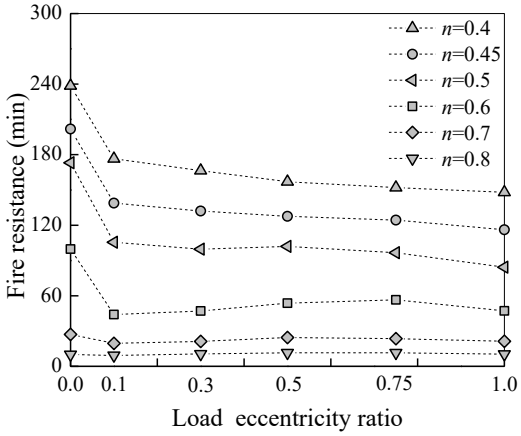

(a) D=400 mm, λ=30

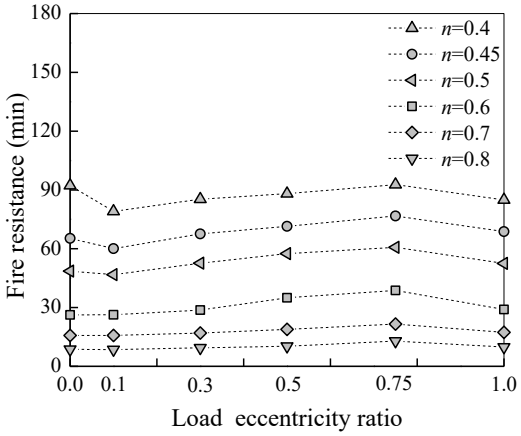

(b) D=400 mm, λ=50

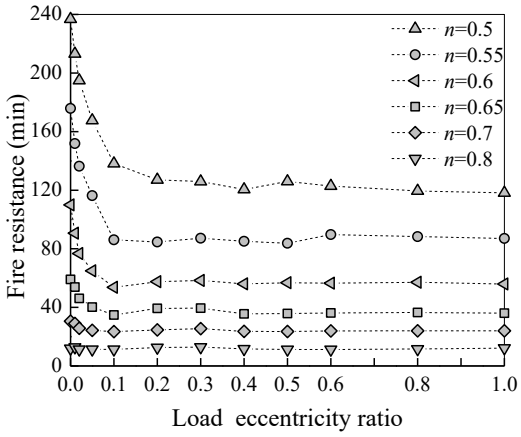

(c) D=600 mm, λ=30

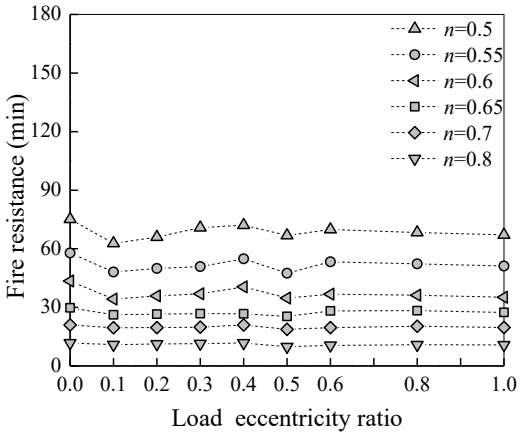

(d) D=600 mm, λ=50

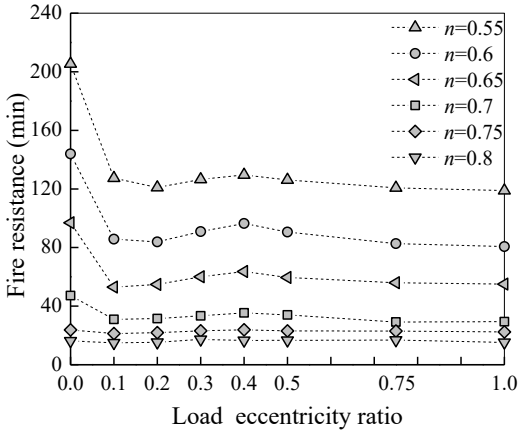

(e) D=800 mm, λ=30

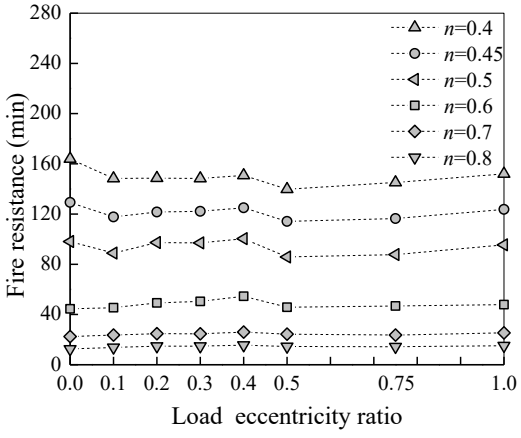

(f) D=800 mm, λ=50

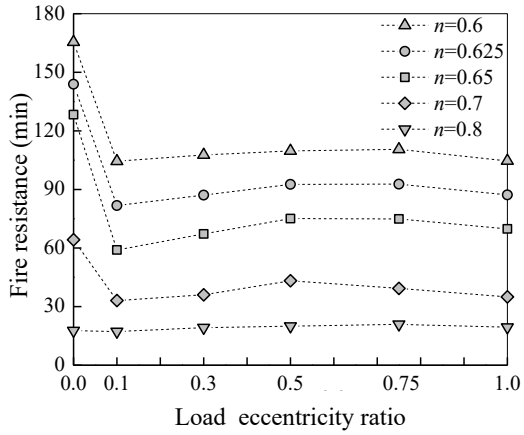

(g) D=1000 mm, λ=30

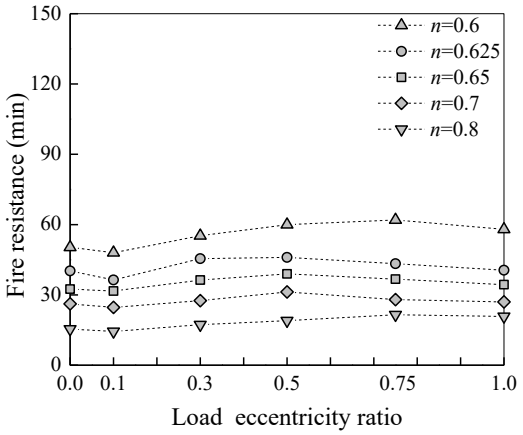

(h) D=1000 mm, λ=50

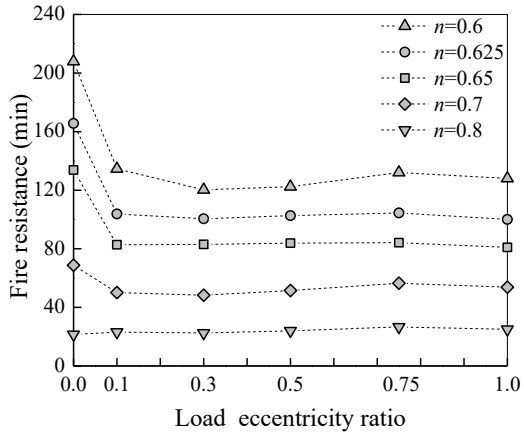

(i) D=1500 mm, λ=30

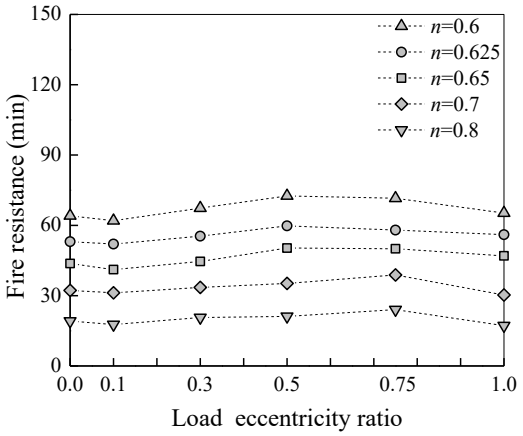

(j) D=1500 mm, λ=50

Fig. 14. Influence of load eccentricity ratio on the fire resistance of unprotected square TRC columns.

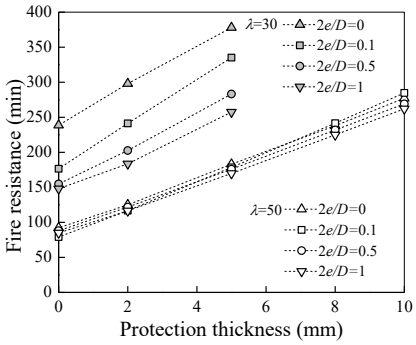

(a) D=400 mm, n=0.4

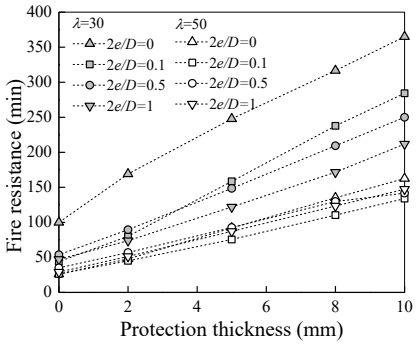

(b) D=400 mm, n=0.6

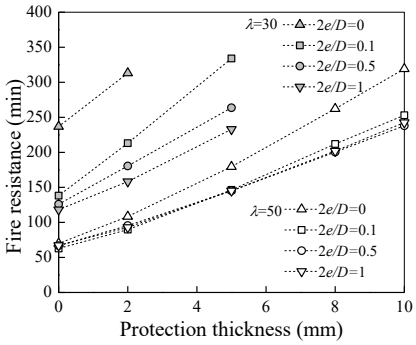

(c) D=600 mm, n=0.5

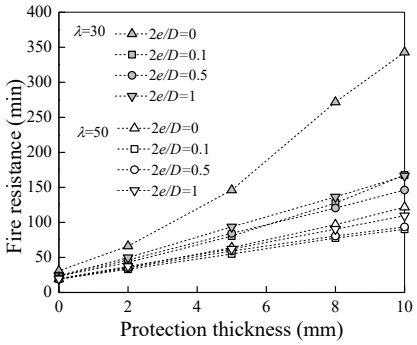

(d) D=600 mm, n=0.7

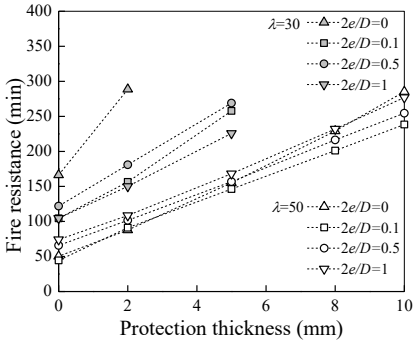

(e) D=1000 mm, n=0.6

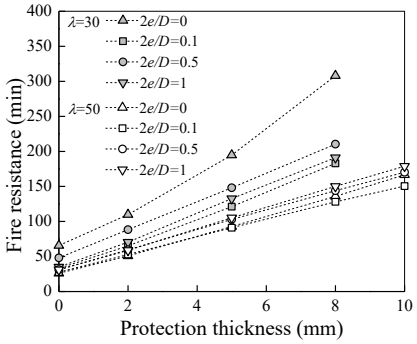

(f) D=1000 mm, n=0.7

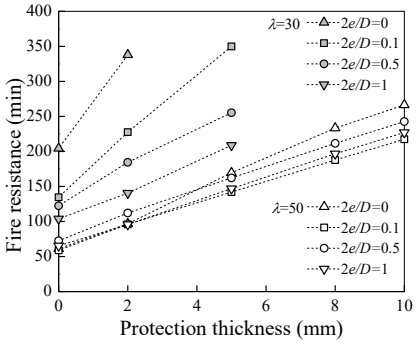

(g) D=1500 mm, n=0.6

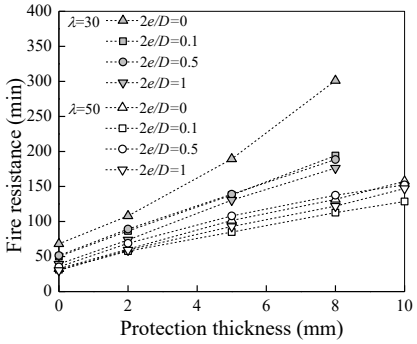

(h) D=1500 mm, n=0.7

Fig. 15. Influences of load eccentricity ratio and fire protection thickness on the fire resistance of protected square TRC columns.

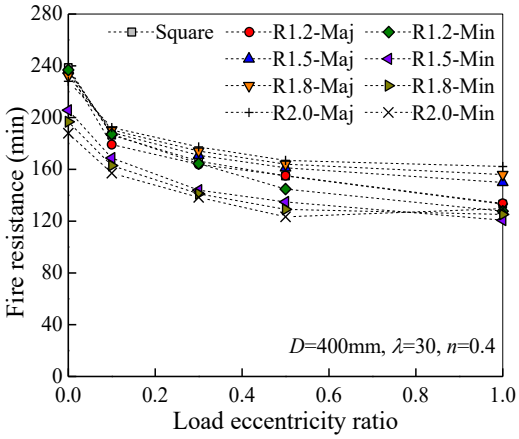

(a) D=400 mm, λ=30, n=0.4

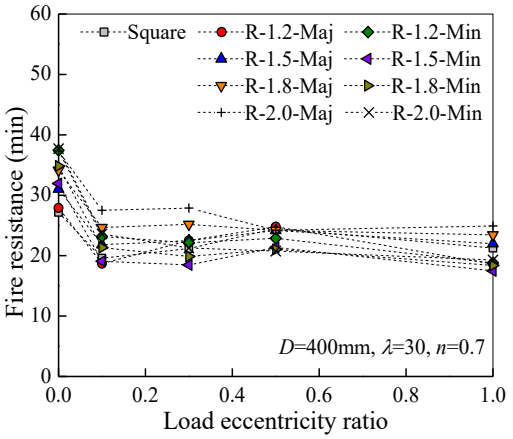

(b) D=400 mm, λ=30, n=0.7

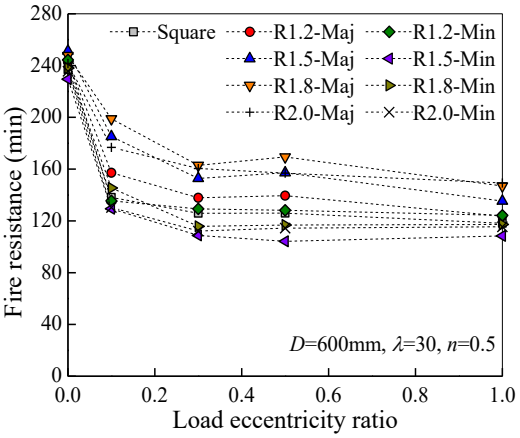

(c) D=600 mm, λ=30, n=0.5

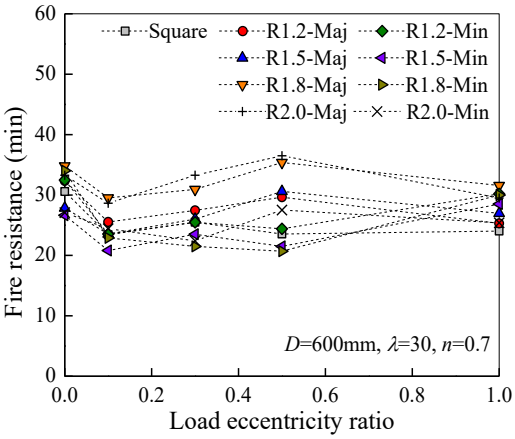

(d) D=600 mm, λ=30, n=0.7

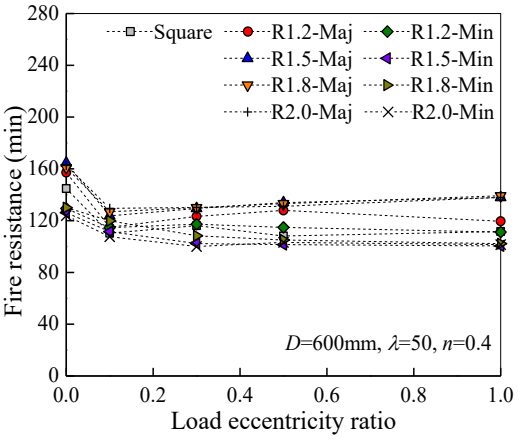

(e) D=600 mm, λ=50, n=0.4

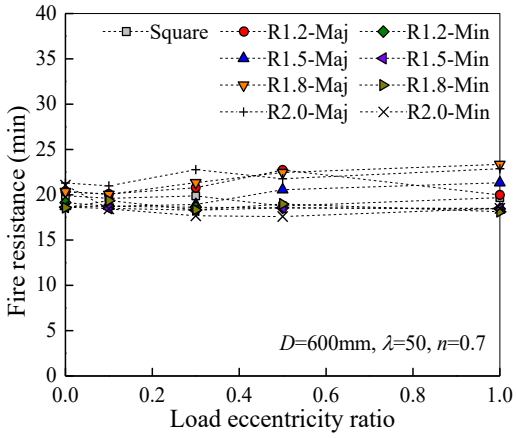

(f) D=600 mm, λ=50, n=0.7

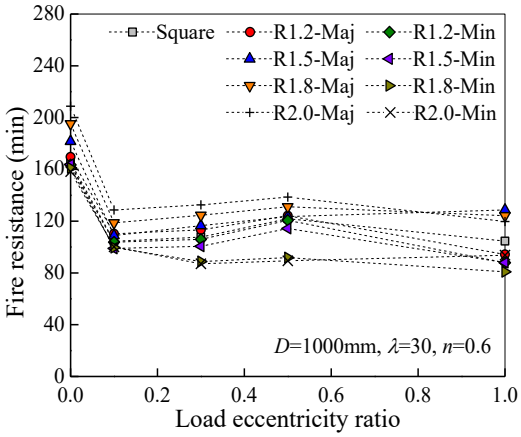

(g) D=1000 mm, λ=30, n=0.6

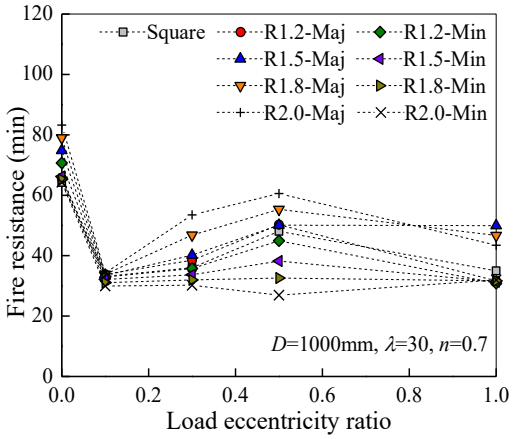

(h) D=1000 mm, λ=30, n=0.7

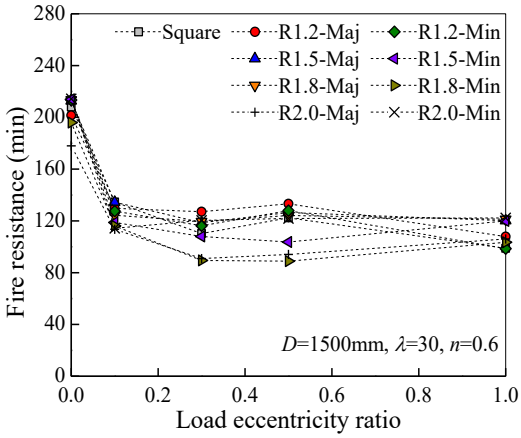

(i) D=1500 mm, λ=30, n=0.6

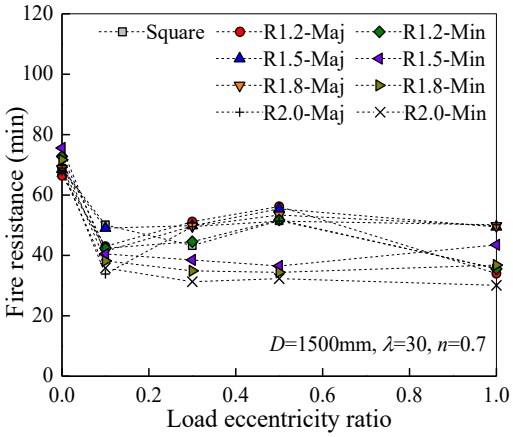

(j) D=1500 mm, λ=30, n=0.7

Fig. 16. Influences of aspect ratio and load eccentricity ratio on the fire resistance of unprotected rectangular TRC columns.

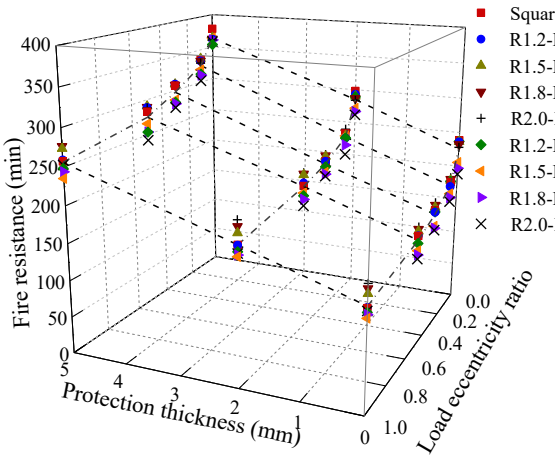

(a) D=400 mm, λ=30, n=0.4

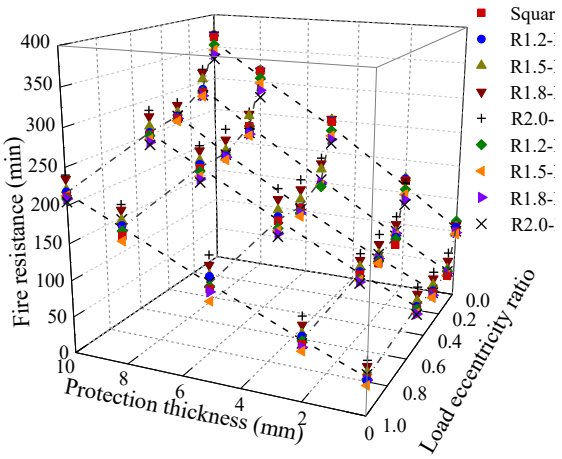

(b) D=400 mm, λ=30, n=0.6

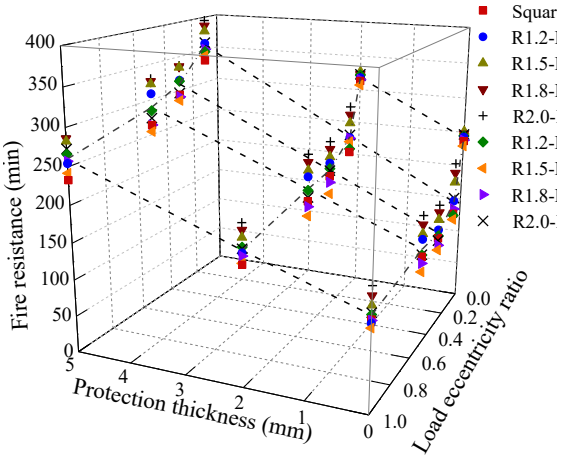

(c) D=600 mm, λ=30, n=0.5

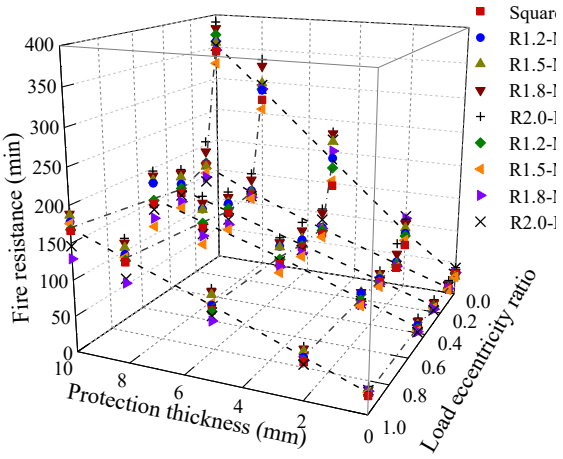

(d) D=600 mm, λ=30, n=0.7

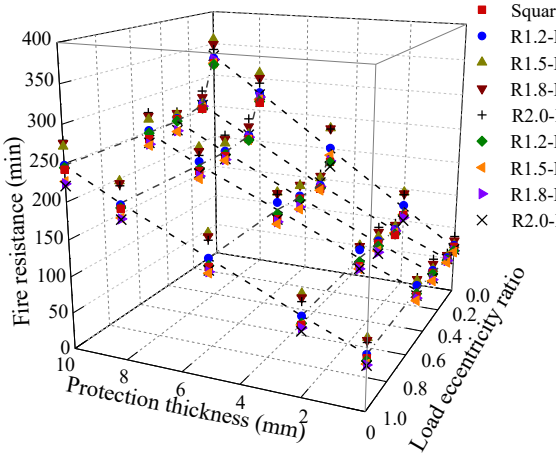

(e) D=600 mm, λ=50, n=0.5

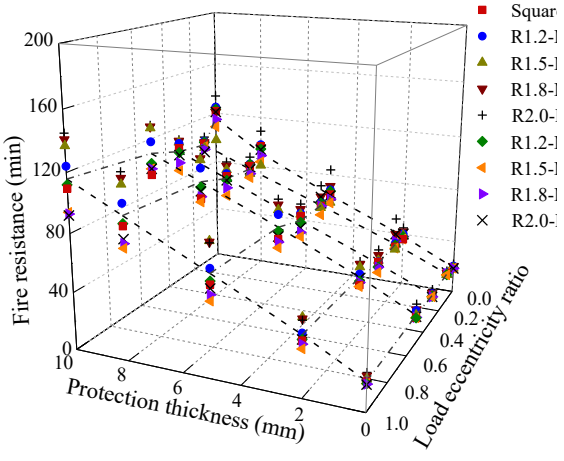

(f) D=600 mm, λ=50, n=0.7

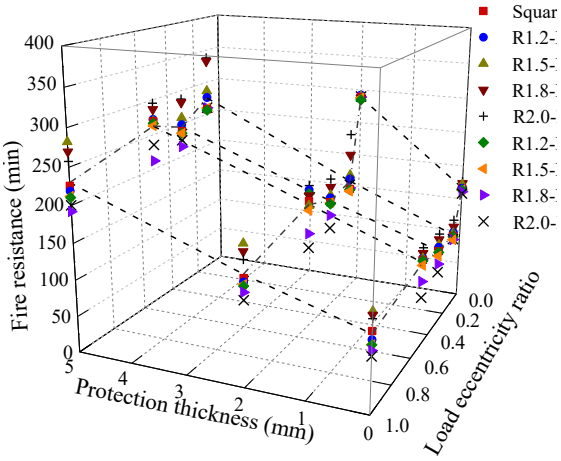

(g) D=1000 mm, λ=30, n=0.6

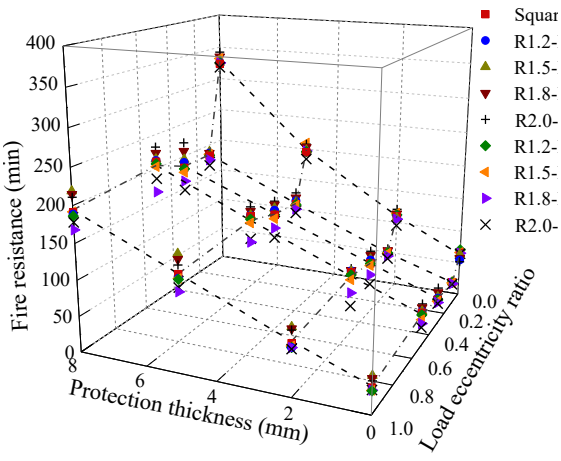

(h) D=1000 mm, λ=30, n=0.7

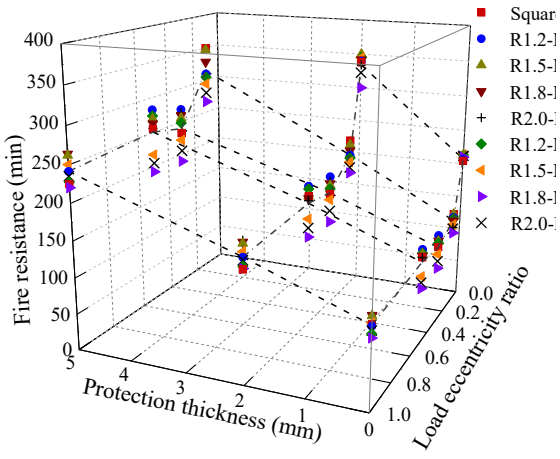

(i) D=1500 mm, λ=30, n=0.6

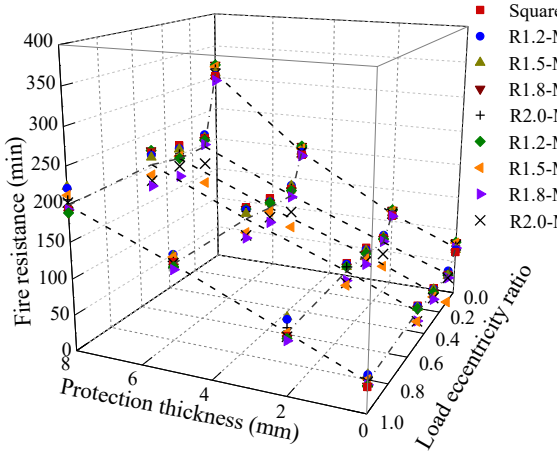

(j) D=1500 mm, λ=30, n=0.7

Fig. 17. Influences of aspect ratio and load eccentricity ratio on the fire resistance of protected rectangular TRC columns.

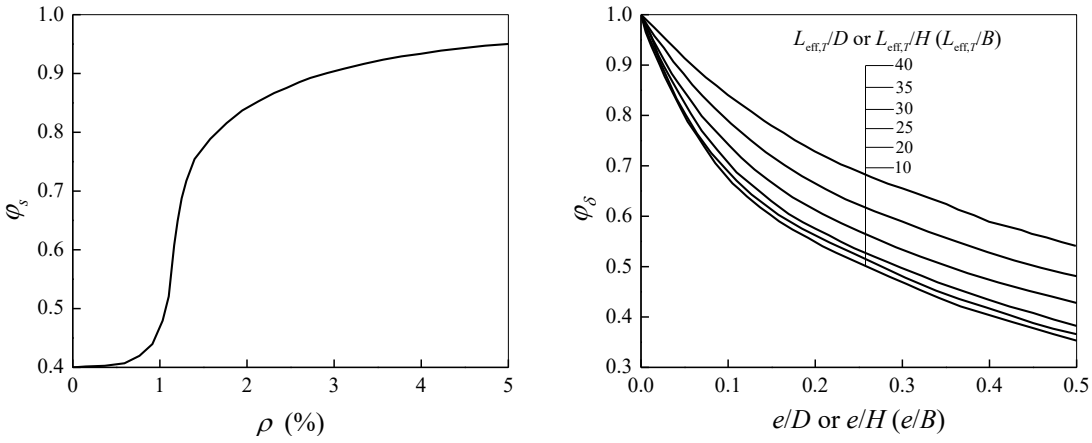

(a) Coefficient φ_s (b) Coefficient φ_δ

Fig. 18. Correction coefficients for the high-temperature buckling resistance under eccentric loading.

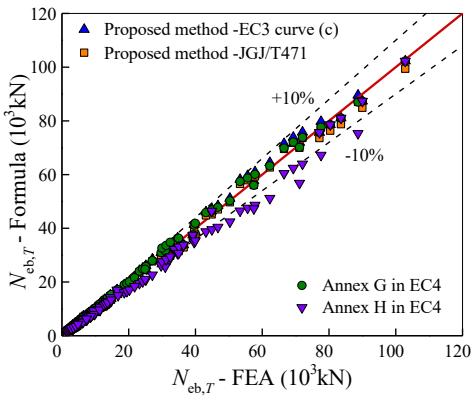

(a) Unprotected square TRC

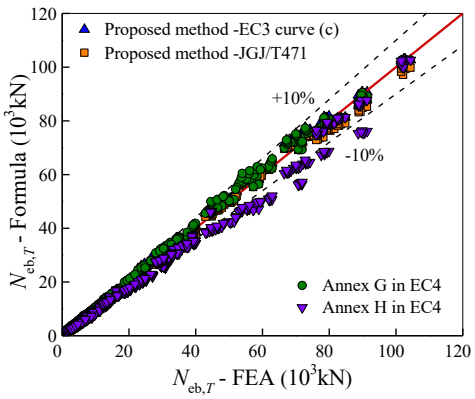

(b) Unprotected rectangular TRC

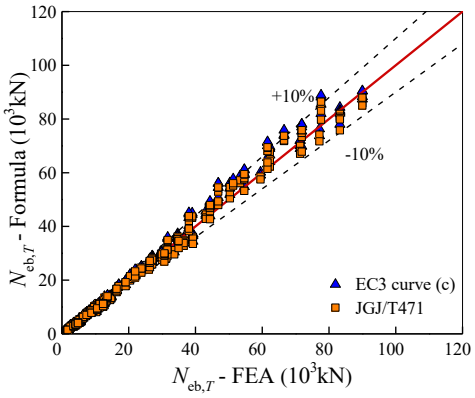

(c) Protected square TRC

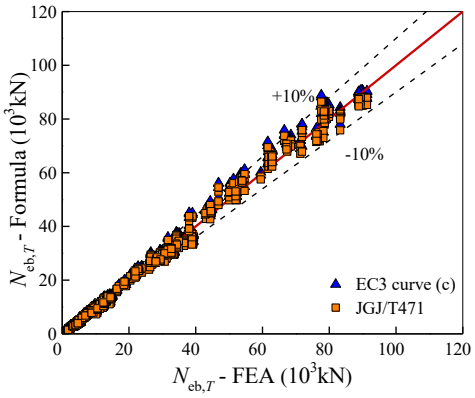

(d) Protected rectangular TRC

Fig. 19. Comparison between the predicted high-temperature buckling resistance under eccentric loading using the proposed method and FEA results.

Table 1. Collected fire test data of eccentrically-loaded CFST columns.

Reference	No.	Section	D or $H\times B$ (mm)	t_s (mm)	$L(L_e)$ (m)	Rebars	BC	f_y (MPa)	f_c' (MPa)	f_b (MPa)	$2e/D$ or $2e/H$ ($2e/B$)	d_p (mm)	N_f (kN)	$t_{FR,t}$ (min)	$t_{FR,p}$ (min)	$t_{FR,p}/t_{FR,t}$	$t_{FR,p}$-$t_{FR,t}$ (min)
Han et al. [43]	R-2	R	300×200	7.96	3.81(3)	-	P-P	341	39.2	-	0.15 (B)	0	2233	24	25.4	1.06	1.4
	R-4	R	300×150	7.96	3.81(3)	-	P-P	341	39.2	-	0.15 (B)	0	1853	20	20.4	1.02	0.4
	SP-3	S	350	7.7	3.81(3)	-	P-P	284	15	-	0.3	7	1670	109	112.7	1.03	3.7
Espinos et al. [44]	S1	S	150	8	3.18(3.04)	4ϕ12	P-P	452.7	45	548	1.0	0	161.13	26	27.7	1.06	1.7
	S2	S	220	10	3.18(3.04)	4ϕ16+ 4ϕ10	P-P	560.3	39.7	527(ϕ16) 575.3(ϕ10)	1.0	0	446.53	23	26.5	1.15	3.5
	S5	S	150	8	3.18(3.04)	8ϕ12	P-P	452.7	48.7	548	1.5	0	133.18	29	31.4	1.08	2.4
	S6	S	220	10	3.18(3.04)	4ϕ20+ 4ϕ16	P-P	560.3	38.8	576(ϕ20) 527(ϕ16)	1.0	0	452.63	29	33.8	1.17	4.8
Espinos et al. [45]	R3	R	250×150	10	3.18(3.04)	-	P-P	428.3	32	-	0.4 (B)	0	374.7	23	24.3	1.06	1.3
	R4	R	250×150	10	3.18(3.04)	4ϕ16	P-P	457.7	36.3	527	1.0 (B)	0	276.9	27	30.1	1.11	3.1
	R5	R	250×150	10	3.18(3.04)	-	P-P	457.7	36.5	-	0.4 (H)	0	456.7	24	25.4	1.06	1.4
	R6	R	250×150	10	3.18(3.04)	4ϕ16	P-P	457.7	32.9	527	1.0 (H)	0	322.1	34	36.4	1.07	2.4
	R9	R	350×150	10	3.18(3.04)	-	P-P	383.3	37.6	-	0.4 (B)	0	540.1	22	25.1	1.14	3.1
	R10	R	350×150	10	3.18(3.04)	4ϕ16+ 4ϕ10	P-P	474	37.3	527(ϕ16) 575(ϕ10)	1.0 (B)	0	383.9	25	26.0	1.04	1
	R11	R	350×150	10	3.18(3.04)	-	P-P	383.3	38	-	0.4 (H)	0	683	22	23.2	1.05	1.2
	R12	R	350×150	10	3.18(3.04)	4ϕ16+ 4ϕ10	P-P	383.3	39.7	527(ϕ16) 575(ϕ10)	1.0 (H)	0	481.4	18	19.2	1.07	1.2

Reference	No.	Section	D or $H\times B$ (mm)	t_s (mm)	$L(L_e)$ (m)	Rebars	BC	f_y (MPa)	f_c' (MPa)	f_b (MPa)	$2e/D$ or $2e/H$ ($2e/B$)	d_p (mm)	N_f (kN)	$t_{FR,t}$ (min)	$t_{FR,p}$ (min)	$t_{FR,p}/t_{FR,t}$	$t_{FR,p}$-$t_{FR,t}$ (min)
Moliner et al. [46]	RC-30-20-20	C	159	6	3.18(3)	4ϕ12	P-F	357.22	39	500	0.252	0	180	47	47.5	1.01	0.5
	RC-30-20-40	C	159	6	3.18(3)	4ϕ12	P-F	357.22	40.38	500	0.252	0	360	24	22.7	0.95	-1.3
	RC-90-20-20	C	159	6	3.18(3)	4ϕ12	P-F	357.22	93.67	500	0.252	0	263.8	48	53.5	1.12	5.5
	RC-90-20-40	C	159	6	3.18(3)	4ϕ12	P-F	386.38	96	500	0.252	0	527.7	22	22.8	1.04	0.8
	RC-30-50-20	C	159	6	3.18(3)	4ϕ12	P-F	315.22	31	500	0.629	0	140	39	37.8	0.97	-1.2
	RC-30-50-40	C	159	6	3.18(3)	4ϕ12	P-F	315.22	39.5	500	0.629	0	279.9	20	21.6	1.08	1.6
	RC-90-50-20	C	159	6	3.18(3)	4ϕ12	P-F	315.22	92.97	500	0.629	0	203.7	40	47.6	1.19	7.6
	RC-90-50-40	C	159	6	3.18(3)	4ϕ12	P-F	315.22	91.87	500	0.629	0	407.4	15	17.5	1.17	2.5
															Mean	1.07	2.11
															Std.dev	0.06	

Notes: "R" rectangular column; "S" square column; "C" circular column; "*D*" sectional dimension of a square or circular column; "*H*" sectional depth of a rectangular column; "*B*" sectional width of a rectangular column; "t_s" thickness of steel tube; "ϕ" diameter of a reinforcing bar; "*L*" whole column length; "L_e" exposed column length; "BC" boundary condition; "P-P" pinned-pinned; "P-F" pinned-fixed; "f_y" steel tube yield strength; "f_c'" concrete cylinder compressive strength; "f_b" reinforcing bar yield strength; "2*e*/*D*" load eccentricity ratio of a square or circular section; "2*e*/*H*" or "2*e*/*B*" load eccentricity ratio of a rectangular section, the letter *H* or *B* in the bracket next to the load eccentricity ratio indicates that the eccentricity is applied along the major axis or minor axis; "d_p" fire protection thickness; "N_f" applied axial load in fire; "$t_{FR,t}$" tested fire resistance; "$t_{FR,p}$" predicted fire resistance.